



NTNU – Trondheim
Norwegian University of
Science and Technology

Condition Assessment of Line Connectors by Current Pulse Measurements

Design and Testing of a Lightweight

Current Pulse Source Prototype

Knut Fandrem

Master of Science in Electric Power Engineering

Submission date: June 2014

Supervisor: Hans Kristian Høidalen, ELKRAFT

Co-supervisor: Svein Magne Hellesø, Sintef Energy Research

Norwegian University of Science and Technology
Department of Electric Power Engineering

Problem Description

Condition assessment of high power apparatus is a necessity for operating a stable power network. Thorough assessments do not only reveal the condition of the apparatus but also estimations of the remaining lifetime. In high power transmission, the power lines are an essential component. The weakest link of a high power transmission line are the line connectors. Thus, it is important that the connectors condition is inspected thoroughly to reveal their condition and remaining lifetime.

A measurement technique previously used to condition assess SF₆ encapsulated connections has been adapted by SINTEF Energy to apply to line connectors. This method should be further developed to better suit condition assessment of line connectors. Tasks conducted in the master thesis:

- Design and construct a new lightweight pulse source based on prior studies on weight reduction by reduced current pulse rise times.
- Validate the design by using the prototype pulse source to condition assess connector samples with a known condition.
- Look into how the design aspects of the prototype handles condition assessment on connector samples with an unknown condition.
- Conduct measurements to investigate aspects of the prototype design not revealed during the condition assessment measurements.
- Make adaptations to the design based on the results from the laboratory measurements.

Assignment given: January 20, 2014

Supervisor: Professor Hans Kristian Høidalen, NTNU

Preface

This thesis is the finalization of a master's degree in Electric Power Engineering at the Norwegian University of Science and Technology (NTNU), and is a part of a larger project conducted by SINTEF Energy AS. The work and studies presented in this report were conducted in the spring semester of 2014, and is within the field of high voltage technology and condition assessment of high voltage apparatus.

Working on this thesis has not only given great insight into the field of laboratory work, but also into prototype design and condition assessment of high voltage components. Being able to work in collaboration with a large research organization as SINTEF Energy has made it possible to explore several field of study during the scope of this thesis, ranging from microcontroller programming to mechanical engineering.

During the course of this project I have received guidance from several contributors both internal and external of NTNU. I would especially like to thank my supervisor professor Hans Kristian Høidalen at NTNU and co-supervisors Svein Magne Hellesø and Magne Runde at SINTEF Energy for their contribution and guidance throughout the project. Their input when discussing the design and testing of the prototype has been of great help. I would also like to thank the staff at the NTNU Service Laboratory and Workshop for their great service minded attitude and willingness to help the students, and for allowing me to use their work place during the construction of the prototype.

Trondheim, 16-06-2014

Knut Fandrem

Abstract

This thesis presents and discusses the development, design and testing of a lightweight current pulse source prototype used for condition assessment of line connectors. The thesis is a continuation of a student project conducted in the fall semester of 2014 with the title "*Condition Assessment of Line Connectors by Current Pulse Measurements - Effect of Reduced Pulse Rise Time And Connection Cable Cross Section*". The student project looked into how weight and size could be removed from the present pulse source design, both by a reduced capacitor bank and by reduced connection cable cross section. The results from this project lead to the development of the lightweight pulse source prototype.

The design and development is divided into three sections. Initially, the overall idea and generalization of the design is presented and discussed. Secondly, based on this conceptualization the design is broken down to each major component. These components were the battery, thyristor, capacitor bank, microcontroller, DC-DC Converter, and user interface. Their function and design criteria are presented and discussed in the thesis. The thesis also presents the circuit schematics of all the components designed specially for the prototype. Finally, the design is summarized and its weight and size compared to the present pulse source design. The measurements show that new pulse source prototype weights 7.6 kg compared to the 35 kg of the old design and is 47 dm³ smaller. Note that the weight is measured without the connection cords and measurement equipment.

One of the major differences beside the size and weight is that the present pulse source uses a hardware based sequence control, while the prototype utilizes a microcontroller. This allows a much more flexible system since the behavior of the sequence control can be altered by rewriting the script. The microcontroller and script are presented in detail in the thesis and in the appendix.

To verify the design, and to look into how the prototype operates during actual condition assessment measurements, a total of thirteen connectors were assessed. Three of these had an already known condition, while for the rest no prior condition assessment existed. The three connectors with a known state showed that it was possible to reproduce the results from the prior measurements using the pulse source prototype. The ten final connectors were meant to increase the number of measurements to see how the prototype handled during actual assessment tests. These measurements show that the prototype only needed a few alterations to it design to operate satisfactory. These alterations are presented and discussed in the thesis, while the condition assessment of all the connectors is presented in the appendix.

In addition to the condition assessment measurements there were also conducted two separate experiments to define the battery capacity and setpoint accuracy of the prototype. The battery capacity test revealed that the battery capacity of the prototype is sufficiently large to supply the unit with power during continuous operation for at least four hours and ten minutes, and deliver 500 consecutive shots. The setpoint accuracy test indicated that the prototype's control sequence was able to reproduce the same current amplitude for the same setpoint with a deviation of only 26.4 A.

All the tests performed on the prototype show that it works and operates as intended. Tests have shown that the prototype is able to produce and reproduce current pulses accurately up to and above 6000 A, and that the microcontroller based sequence control functions as intended.

Sammendrag

Denne masteroppgaven presenterer og diskuterer utviklingen og testingen av prototypen på en lettvekts strømpulskilde brukt til tilstandskontroll av linjeskjøter. Prosjektet er en videreføring av studentprosjektet, "*Condition Assessment of Line Connectors by Current Pulse Measurements – Effect of Reduced Pulse Rise Time and Connection Cable Cross Section*", som ble gjennomført i høstsemesteret 2013. Prosjektet undersøkte hvordan vekten og størrelsen på den nåværende strømpulskilden kunne reduseres ved reduksjon av kildens kondensatorbank og ved reduksjon av tilkoblingsledningenes tverrsnitt. Det er resultatene fra dette prosjektet som har ført til utviklingen av den nye lettvekts strømpulskilden.

Utviklingen er delt opp i tre seksjoner. Først er en konseptualisering av prototypens overordnede design og virkemåte presentert og diskutert. Basert på denne overordnede ideen er hver av prototypens hovedkomponenter presentert, og deres dimensjoneringskriterier diskutert. Disse komponentene er batterikilden, tyristoren, kondensatorbanken, mikrokontrolleren, DC-DC omformerer og brukergrensesnittet. Rapporten presenterer også koblingskjemaene til alle komponentene som ble spesielt designet for prototypen. Til slutt presenteres det ferdigstilte designet og prototypens vekt og størrelse blir sammenlignet med det nåværende pulskilde designet. Målingen viser at prototypen veier 7.6 kg. Til sammenligning veier den nåværende pulskilden nesten 35 kg. I tillegg er størrelsen betraktelig redusert. Vekten er målt uten tilkoblingsledninger og det eksterne måleutstyre

En av de største forskjellene sett bort fra størrelsen og vekten er at mens den nåværende pulskilden benytter en hardware basert sekvenskontroll, benytter prototypen en mikrokontroller. Dette gir en mye større fleksibilitet siden sekvensen kan endres ved å skrive om mikrokontrollerscriptet. Mikrokontrolleren og scriptet benyttet i prototypen er beskrevet i detalj både i rapporten og appendikset.

For å verifisere virkemåten og for å undersøke hvordan prototypen håndterer faktiske tilstandskontrollmålinger ble tilstanden på tretten linjeskjøter undersøkt. Tre av disse hadde en allerede kjent tilstand, mens for de resterende ti eksisterte ingen foranliggende tilstandskontroll. Målingene på de tre skjøtene med kjent tilstand viste at det var mulig å reprodusere resultatene fra de tidligere målingene ved å benytte pulskildeprototypen. De siste ti skjøtene ble benyttet til å øke antall målinger for å se hvordan prototypen håndterte faktiske tilstandskontrollmålinger. Disse målingene viste at prototypen kun trengte små modifikasjoner for å fungere tilfredsstillende. Disse endringene er presentert og diskutert i rapporten, mens resultatene fra tilstandskontrollen av alle skjøtene finnes i appendikset.

I tillegg til tilstandskontrollmålingene ble det utført to separate forsøk for å definere pulskildens batterikapasitet og setpunktsnøyaktighet. Batterikapasitetsmålingene viste at prototypens batterikapasitet er tilstrekkelig til å forsyne enheten i minst fire timer og ti minutter, og produsere 500 påfølgende «skudd». Målingene gjort på setpunktsnøyaktigheten viste at prototypens sekvenskontroll var kapabel til å reproducere den samme størrelsen på strømmen for det samme setpunktet med et standard avvik på 26.4 A.

Alle testene som ble gjennomført på prototypen viser at designet virker som tiltenkt. Tester har vist at pulskildeprototypen kan produsere og reproducere strømpulser nøyaktig opp til 6000 A, og at den mikrokontrollerbaserte sekvenseringen fungerer som tiltenkt. Vektreduksjonen sammenlignet med den nåværende pulskilden er på 28 kg, og størrelsen er redusert med nesten 47 dm³.

Contents

Problem Description	i
Preface	ii
Abstract	iv
Sammendrag	vii
List of Figures	xiv
List of Tables	xv
1 Introduction	1
1.1 Motivation	1
1.2 Objectives	2
1.3 Report Structure	3
2 Theory and Background	5
2.1 Electrical Contact Theory	5
2.1.1 Contact Surface and Contact Spots	5
2.1.2 The Constriction Resistance	6
2.1.3 Degradation of Stationary Contacts	8
2.1.4 Connector Degradation Pattern	9
2.1.5 Contact Spot Temperature	9
2.1.6 Thermal Response	11
2.2 Overhead Line Connectors	13
2.2.1 General Description	14
2.2.2 Failure Modes	14
2.3 Methods for Condition Assessment of Line Connectors	15
2.3.1 Visual Inspection	15
2.3.2 Thermal Imaging	16
2.3.3 Resistance Measurements	16
2.3.4 Comparison of Resistance Measurements and Thermal Imag- ing	18
2.4 Current Pulse Measurements	19
2.5 Mathematical Model	21
2.6 Condition Assessment Criteria	23
3 Prior Studies	25
3.1 Weight Reduction by Reduced Pulse Lengths	25
3.1.1 Measurement Setup	25
3.1.2 Results and Conclusion	26

3.2	Reduced Connection Cable Cross Section	26
3.2.1	Mathematical Analysis	27
3.2.2	Laboratory Measurements	28
4	Current Pulse Source Prototype	29
4.1	Principle of Operation	29
4.2	User Interface	32
4.3	The Prototype's Major Components	33
4.3.1	Capacitor Bank	33
4.3.2	Power Source	34
4.3.3	Thyristor	38
4.3.4	DC-DC Converter	39
4.3.5	Microcontroller Unit	41
4.4	Sequence Control	43
4.5	Sequence Control Circuits	43
4.5.1	Thyristor Trigger Signal	44
4.5.2	DAQ-card Trigger Signal	45
4.5.3	Voltage Measurement Circuit	46
4.6	Final Design	48
5	Condition Assessment Tests	51
5.1	Connector Samples	51
5.1.1	The French Connectors	51
5.1.2	The Finnish Connectors	52
5.2	Methods	53
5.2.1	Equipment	53
5.2.2	Measurement Setup	54
5.2.3	Measurement Procedure	55
5.3	Results and Discussion	57
5.3.1	The French Connectors	57
5.3.2	The Finnish Connectors	61
5.4	Increased Pulse Rise Time	61
5.5	Resistance Increase Error at Low Current Magnitudes	63
6	Prototype Functionality Tests	69
6.1	Battery Lifetime	69
6.1.1	Equipment and Measurement Setup	69
6.1.2	Results and Discussion	70
6.2	Setpoint Accuracy	71

6.2.1	Equipment and Measurement Setup	71
6.2.2	Results and Discussion	73
6.3	Alteration to the Prototype Design	73
7	Conclusion and Further Work	75
7.1	Conclusion	75
7.2	Further Work	76
	References	77
	Appendix	
	Appendix A - Condition Assessment	I
	Appendix B - Microcontroller Script	XV
	Appendix C - Circuit SchematicsXIX
	Appendix D - Component ListXXIII
	Appendix E - ACSR Product Catalog	XXV

List of Figures

- 2.1 Illustration of the electrical contact between two surfaces. 6
- 2.2 Illustration of the distribution and shape of the mechanical and electrical contact spots on the apperent contact surace. 7
- 2.3 Connector degradation pattern. 10
- 2.4 Relationship between voltage drop and temperature for a symmet-ric contact spot between two aluminum interfaces. 11
- 2.5 Temperature development as a function of time. 12
- 2.6 Thermal response time as a function contact spot size. 13
- 2.7 Principle schematic of an ACSR line connector. 14
- 2.8 Resistance ratio measurements. 17
- 2.9 Comparison of the $R(I)$ -characteristic for a very good and poor line connector. 20
- 2.10 Principle schematic of the current pulse source. 20
- 2.11 Pulse circuit model. 21
- 2.12 Estimation of the current pulse. 23

- 3.1 Current vs. resistance relationship with different pulse rise times for a good and very good line connector. 26
- 3.2 The normalized current pulse amplitude as a function of conductor cross section for different values of capacitance. 27
- 3.3 Comparison of current pulse amplitude for different values of ca-pacitance with normalized values. 28

- 4.1 Principle schematic of circuit operation. 30
- 4.2 Idealized charging scheme. 31
- 4.3 Proposed user interface. 33
- 4.4 Comparison of critical rise time and measured current pulse. . . . 39
- 4.5 External bias (Ex.B) control scheme. 40
- 4.6 Schematic of the DC-DC converter control circuit. 41
- 4.7 An Arduino Uno R3. 42
- 4.8 Sequence diagram for the measurement sequence. 44
- 4.9 Schematic of the thyristor trigger signal circuit. 45
- 4.10 Schematic of the DAQ-card trigger signal circuit. 46
- 4.11 Schematic of the voltage measurement circuit. 47
- 4.12 Picture of the prototype’s final design. 49

5.1	A picture of one of the Finnish Connectors.	52
5.2	An illustration of reference system used on the Finnish Connectors.	53
5.3	Measurement setup for the prototype condition assessment tests. . .	55
5.4	Measurement procedure flow chart.	56
5.5	Longer conductor side of Connector 1.	58
5.6	Longer conductor side of Connector 11.	59
5.7	Shorter conductor side of Connector 6.	60
5.8	Comparison of the current pulse produced by the pulse source prototype and the previous 10 mF pulse.	62
5.9	Current pulse comparison for the longer side of Connector 11 and the shorter side of Connector 6.	63
5.10	$R(I)$ -plot of connectors in a very good condition with and without increase in the resistance at low currents.	64
5.11	$R(I)$ -plot of connectors in a very good condition showing the difference in increased resistance at low current magnitudes.	65
5.12	Modified measurement plot for side B of FIN10.	66
5.13	Comparison of the increase in measured resistance with increas- ing current at low current magnitudes for different measurement techniques.	67
6.1	Measurement setup for the battery life time test.	70
6.2	Setpoint accuracy measurement setup.	72

List of Tables

2.1	Recommended maintenance due to resistance ratio measurements and thermal imaging.	18
4.1	Values for different capacitor bank setups.	34
4.2	The pulse source prototype's physical properties.	49
5.1	Technical data for an Ostrich conductor.	52
6.1	Results from the battery capacity test.	71
6.2	Results from the battery capacity test.	73

1 Introduction

The aim of this thesis is to design, construct and test a lightweight current pulse source prototype used to condition assess overhead line connectors. The development conducted during the duration of this project is based on the findings of previous studies done on weight reduction on current pulse batteries.

1.1 Motivation

Condition assessment of high voltage equipment is not only performed to evaluate the condition of the equipment, but also to try to estimate its remaining lifetime. This is done to avoid unexpected failures, with consequences ranging from small voltage dips to large blackouts. Such failures often become expensive, depending on the severity and location of the failure, not only to the customer, but also to the utility. This gives an extra incentive to monitor the condition of the different components in high voltage networks. Today it is mostly common to monitor the large and expensive apparatus like transformers, generators, and switching equipment, but also unexpected failures in the less expensive equipment may have large consequences. Line connectors are often the weakest link in a high voltage transmission line and an unexpected failure to such a component may have large consequences, especially for the largest transmission voltages. Thus, it is important that also connectors undergo some sort of condition assessment to reveal their condition and remaining lifetime.

There are several ways to condition assess line connectors, spanning from simple visual inspection to more elaborate systems like x-ray imaging. The most common method is to use an infrared camera to pick up the thermal radiation emitted by the connector. The reason why this is so popular, is that large portions of a power line can be assessed quickly by mounting a thermal imaging camera to a helicopter. Even though this method is quick, it has on several occasions been proven inaccurate by line connectors failing shortly after inspection [1]. Since thermal imaging can be interfered by the ambient conditions, unexperienced users might easily detect radiation reflected on the surface of the connector, or fail to take into consideration differences in the external properties of the line connector, like moisture and pollution. Thus, a quick and efficient way of condition assessing line connectors is needed.

A method earlier used to condition assess connections inside encapsulated SF₆ equipment has been adapted to apply for line connectors as well. This method

utilizes a capacitor bank to produce current pulses with a given rise time. Based on contact theory and empirical measurements it can be shown that a connector's resistance changes as a function of the current ($R(I)$), dependent on the condition of the connector. Thus, it is possible to condition assess a connector by sending a series of current pulses with increasing current amplitude through the connector, while measuring the voltage drop.

1.2 Objectives

In the fall of 2013 work was conducted to investigate the possibilities of reducing the weight of the present pulse source design, to create a portable and lightweight pulse source. The work conducted in this thesis is a continuation of the specialization project "*Condition Assessment of Line Connectors by Current Pulse Measurements - Effect of Reduced Pulse Rise Time and Connection Cable Cross Section*". This study will from here on out be referred to as the specialization project.

The aim of this thesis is therefore to utilize the finding of the specialization project to design, construct and test a new light weight pulse source prototype. The testing will be conducted in the NTNU laboratory both on connector samples with a known condition and new connector samples provided by Fingrid. The problem of the thesis can be broken down to five objectives.

1. Design and construct a new lightweight pulse source based on prior studies on weight reduction by reduced current pulse rise times.
2. Validate the design by using the prototype pulse source to condition assess connector samples with a known condition.
3. Look into how the design aspects of the prototype handles condition assessment on connectors samples with an unknown condition.
4. Conduct measurements to investigate aspects of the prototype design not revealed during the condition assessment measurements.
5. Make adaptations to the design based on the results from the laboratory measurements.

1.3 Report Structure

The thesis is divided into seven chapters. The initial two chapters presents the motivation for the conducted study and explains the basic theory behind contact interfaces and condition assessment of contacts. In addition the second chapter presents and discusses several methods for condition assessment of line connectors. After the theory and background is explained, a short summary of the prior studies performed on this subject is presented. The forth chapter presents the calculations and considerations performed when designing the current pulse source prototype. This chapter is followed by two chapters explaining the different measurements and tests used to verify the design, including sections what present and discuss the major findings. The final chapter concludes the results and presents ideas for further development.

All the results from the different measurements are presented in the appendix.

2 Theory and Background

To understand the results and discussion presented in this thesis it is necessary to have a basic understanding of electrical contact theory. This chapter explains the basic principles behind contact theory and the composition of electrical contacts. In addition, a presentation of different condition assessment methods for overhead line connectors is made, including a more thorough description of the current pulse method.

2.1 Electrical Contact Theory

The purpose of an electrical contact is to allow the current to flow from one interface to another. These electrical contacts are usually the weakest link when it comes to the load carrying capability of the system. This section explains the different factors that determine the state and behavior of an electrical contact.

2.1.1 Contact Surface and Contact Spots

On a micro scale level all surfaces are rugged. This means that if two apparently smooth surfaces are pushed together, the area of true contact is smaller than the apparent contact surface. In addition, an oxide film will form on the surface of any metal exposed to air. The oxide films are often insulating, so for a current to flow the oxide layer needs to be punctured. This reduces the electrical contact to the areas where there is mechanical contact between the two surfaces and the mechanical forces have been adequate to puncture the oxide film and create a contact spot (a-spot). This mechanism is illustrated in Figure 2.1. Object A and B with an apparent smooth surface are pushed together to form an electrical contact. The magnification shows that the microscale surface is not smooth and that contact spots have only formed where there is mechanical contact, and where the mechanical force has been adequate to puncture the oxide layer. As shown the current is only able to flow through these contact spots, reducing the effective conductive area, and increasing the current density of the contact surface.

As a result of the unpredictability of the micro scale roughness, there is an uneven distribution of contact spots. This distribution together with the number, shapes and sizes are what determines the electrical properties of the contact. An illustration of the distribution and shapes of the mechanical and electrical contact spots on the apparent contact surface is presented in Figure 2.2 [2].

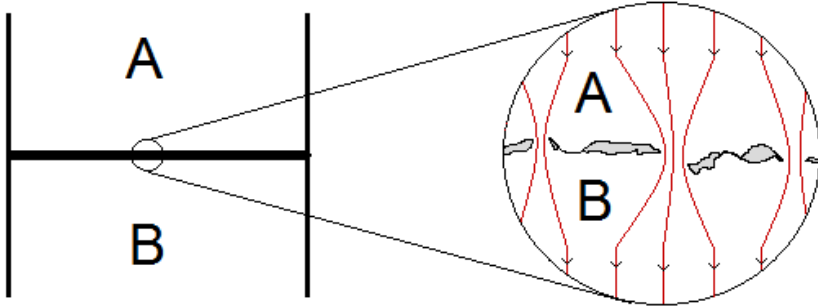


Figure 2.1: Illustration of the electrical contact between two surfaces.

2.1.2 The Constriction Resistance

The resistance between two interfaces is not just the sum of the resistance between the measurement points and the resistance of any surface layers. As mentioned the contact spots reduce the apparent contact surface and thereby increase the current density in the actual contact interfaces. This sudden increase in current density forms an additional electric resistance called the constriction resistance. In *Electric Contacts: Theory and Application* [3] R. Holms presents the following formula for the constriction resistance of a circular monometallic contact spot in a plane interface between to infinitely large electrodes;

$$R = \frac{\rho}{2a} \quad (2.1)$$

where ρ is the resistivity of the material and a is the contact spot radius. Though this formula may seem generic it has been experimentally proven by R. Holm and Störmer [3].

In actual electrical connections, one single contact spot is highly unlikely. The contact interface therefore consist of several parallel contact spots. If the distance between the contact spots is much larger than their diameter, which is quite likely, an approximation of the constriction resistance can be found by considering the contact spots as resistances connected in parallel. By considering a multispot system where the following relationship $A_{ss} = n \cdot A_{ms}$ between the single spot area

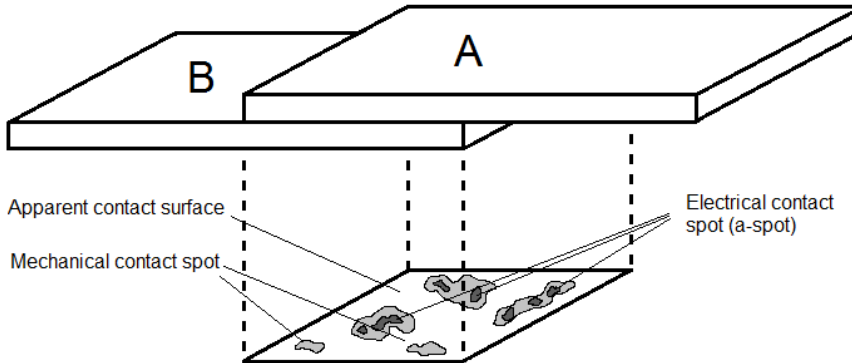


Figure 2.2: Illustration of the distribution and shape of the mechanical and electrical contact spots on the apparent contact surface.

(A_{ss}) and multispot area (A_{ms}) is true. The relationship between the constriction resistance of the singlespot system (R_{ss}), and the constriction resistance of the multispot system (R_{ms}) becomes;

$$R_{ss} = \sqrt{n} \cdot R_{ms} \quad (2.2)$$

where n is the number of contact spots in the multispot interface. If (2.3) is inserted into (2.1) one finds the following formula for the constriction resistance of a multispot system;

$$R_{ms} = \frac{\rho}{2a \cdot \sqrt{n}} = \left(\frac{\rho^2}{4a^2 \cdot n} \right)^{\frac{1}{2}} \quad (2.3)$$

Note that in a real connector the number, shape, size and distribution of the contact spots is hard, if not impossible, to determine. The equation above is therefore meant as a general description of a contact's behavior rather than a tool to calculate its resistance.

2.1.3 Degradation of Stationary Contacts

As the contact ages the contact spots are reduced in size and will eventually vanish, reducing the conducting area of the contact. The physical mechanisms that cause this degradation are only partly clarified [2]. Below some of the most common degradation mechanisms are explained.

As mentioned, all metals exposed to air will undergo a constant oxidation and corrosion process, which will deteriorate contact spots over time. The corrosion process may also increase the pressure inside the contact, thus reducing the mechanical force between the interfaces [1]. Contacts placed in a humid or other ways corrosive environment are more vulnerable than contacts placed in a dry and clean environment.

Another known factor that contributes to contact spot degradation is fretting. Fretting occurs due to tiny, cyclic, lateral movements between the contact interfaces. These arise due to vibrations caused by the system frequency, thermal expansion or contraction caused by temperature variations, or other external sources. The movement erodes and wears down the surface causing small particles to appear on the surface. These oxidize and remain between the contact interfaces preventing proper electrical contact [2][1].

In the interface between to different metals, different metallurgical processes may form alloys. The electrical conductivity of such alloys are usually quite poor compared to the base metal. As an example, an alloy consisting of 20 % aluminum and 80 % copper only has 6 % of the conductivity of pure copper. In addition to the creation of alloys, the difference in electrochemical potential together with humidity may set up currents. These currents create a rapid degradation due to galvanic corrosion. Therefore, contacts between different metals should be avoided [2].

There is seldom only one degradation mechanism contributing to the deterioration of electrical contacts, it is therefore more plausible that a combination of the factors described above causes the aging and degradation of stationary contacts. Also, while one mechanism may be the governing factor, other mechanisms may come in to play as a result of the first, to further accelerate the deterioration process.

2.1.4 Connector Degradation Pattern

As already mentioned the degradation of a line connector stems from the deterioration of the contact spots. If the resistance of a connection interface is measured over time, a common degradation pattern is revealed [4]. This pattern shows that the initial degradation rate is very small, and almost undetectable. This initial phase is then followed by a slight, but steady increase in the resistance until the final phase sets in with a rapid increase. In *Origin, Detection and Cost of Connector Degradation in Electrical Transmission And Distribution systems* R.S. Timist applies Equation (2.3) as a model for this degradation pattern. In actual connection interfaces it is not possible to measure the constriction resistance alone, and a portion of the bulk resistance (R_{bulk}) on each side of the interface must be added. Hence, in the absence of electrically insulating surface films, the contact resistance could be expressed as;

$$R_t = R_{ms} + 2R_{bulk} \quad (2.4)$$

By inserting (2.3) into (2.4) the total resistance becomes a function of the number of contact spots. If one assumes that a system created by mating two aluminum surfaces creates a 1000 equal contact spots with a radius $a = 50\mu\Omega$, and that the measurements are conducted a distance away from the connection interface that give a $R_{bulk} = 5\mu\Omega$, it is possible to plot R_t as a function of the number of contact spots. This is presented in Figure 2.3. The plot is made with the assumption that one contact spot degrades each day. There is one important feature to note from Figure 2.3, and that is the insensitivity of the total connection resistance to the number of contact spots. It is not until approximately 90 % of the contact spots have been lost to degradation that the increased constriction resistance becomes noticeable. This illustrates how difficult it might be to detect connection degradation in the field since a noticeable increase in the contact resistance does not occur until most contact spots have been degraded and lost.

2.1.5 Contact Spot Temperature

In all systems conducting a current, power is dissipated. The power dissipated is proportional to the resistance of the system. For a contact used in electric power systems the contact spot resistance is usually in the microohm-range ($\mu\Omega$ -range) and the power dissipation is thus very small. In spite of the size of the

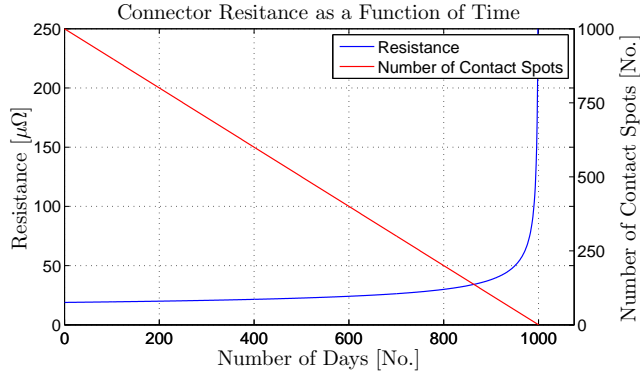


Figure 2.3: Connector degradation pattern.

power dissipation the temperature increase in the contact spot might become significantly large, since the mass of the contact spot is also very small.

In *Electric Contact - Theory and Application* [3], R. Holm presents the contact spot temperature increase as a function of the voltage drop. The relationship between the voltage drop and contact spot temperature is presented in (2.5),

$$T_{max}^2 - T_0^2 = \frac{U^2}{4L} \quad (2.5)$$

where U is the voltage drop across the contact, T_0 is the ambient temperature, T_{max} is the maximum temperature of the contact spot, given in Kelvin, and L is a material constant. The equation assumes a symmetric contact eg. both contact interfaces are of the same isotropic material¹ and the temperature distribution is symmetric around the interface. Figure 2.4 shows the temperature/voltage relationship for a contact at room temperature ($T_0 = 20^\circ\text{C}$) and $L = 2.4 \times 10^{-8} \text{ V}^2/\text{K}^2$. The plot shows that the temperature is nonlinear for low voltages. This is important to note since the resistance is temperature dependent and this may lead to a nonlinear relationship between the current and contact resistance depending on the condition of the connector.

If the current passing through the contact is sufficiently high, or the contact resistance is high, the voltage drop may generate a local temperature increase

¹A material with identical values of a property in all directions.

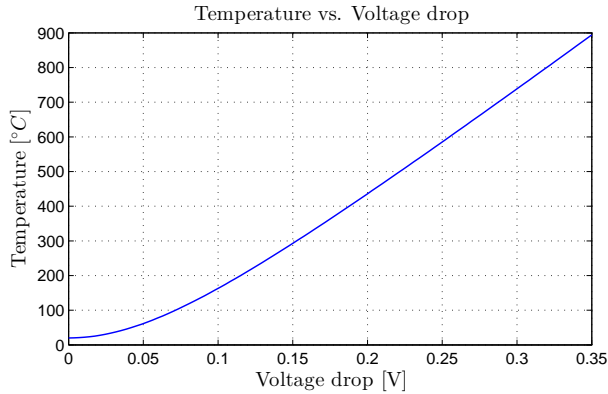


Figure 2.4: Relationship between voltage drop and temperature for a symmetric contact spot between two aluminum interfaces.

that exceeds the metals melting point. This voltage drop level is referred to as the “melting voltage” and for aluminum melting occurs at about 300 mV. Melting usually alters the shape of the contact spot and therefore creates an irreversible change in the contact resistance. The contact resistance may increase or decrease after melting [5].

2.1.6 Thermal Response

As stated earlier the size of the contact spots is often very small, hence the mass of a contact spot is also very small. This allows the temperature of the contact spots to change rapidly compared to the conducting objects adjacent to the connecting interface. Figure 2.5 presents a sketch on how the median temperature of a symmetrical contact spot will develop if a current starts to flow at $t = 0$ [3] [6]. The sketch shows how the normalized temperature (θ) of the contact spot changes as a function of time, represented by the dimensionless variable τ . The relationship between t and τ is presented in the following equation;

$$\tau = \frac{\lambda}{ca^2}t \quad (2.6)$$

where c is the heat capacity of the material, λ is the thermal conductivity, and a is the radius of the contact spot. The maximum temperature ($\theta = 1.0$) is governed by the voltage drop, and is expressed by (2.5).

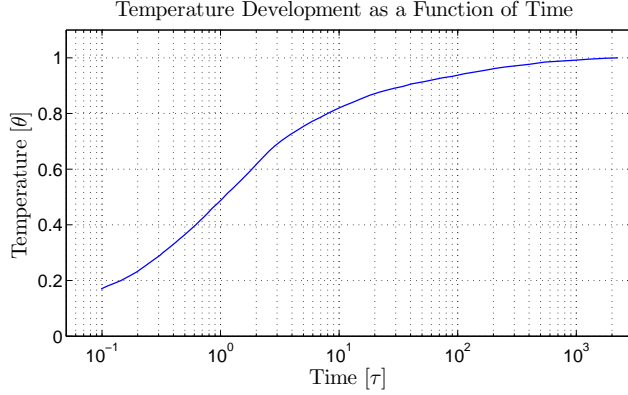


Figure 2.5: Temperature development as a function of time.

Though the relationship between τ and t is known the complexity and randomness of the contact spots in a real system, makes it impossible to accurately calculate. Therefore only an estimation based on the resistance is possible. An approach to this is to calculate the time it will take a contact spot to reach a certain τ .

If (2.4) is solved with regards to a one gets the following expression for the contact spot size;

$$a = \frac{\rho}{2\sqrt{n}(R_t - 2R_{bulk})} \quad (2.7)$$

By inserting (2.7) into (2.6) and solving for t , it is possible to derive an equation for the thermal response time as a function of the number of contact spots and τ ;

$$t = \left(\frac{\rho}{2\sqrt{n}(R_t - 2R_{bulk})} \right)^2 \frac{c}{\lambda} \tau \quad (2.8)$$

Since the aim of this deduction is to see how the thermal response time changes as a function of the contact spot size, a reasonable value for τ must be chosen.

Typically, a system's time constant is the time it takes for the systems step response to reach $1 - 1/e \approx 63.2\%$. Thus, the value of τ corresponding to $\theta = 0.63$ is chosen. From Figure 2.5 we see that this value is reached at about $\tau = 2$.

A typical resistance value for R_t is $58.8 \mu\Omega$ [7]. By inserting this into (2.8), and assuming $R_{cond} = 5.0 \mu\Omega$, it is possible to calculate the thermal response time as function of the contact spot size. The results from this is presented in Figure 2.6.

As Figure 2.6 illustrates, the thermal response time increases asymptotically as the number of contact spots approaches zero, but even for systems with few and large contact spots the thermal response time is in the *ms*-range. This indicates that in most contact interfaces, the contact spot temperature should be able to follow rapid changes in the temperature caused by a change in the contact spot voltage drop.

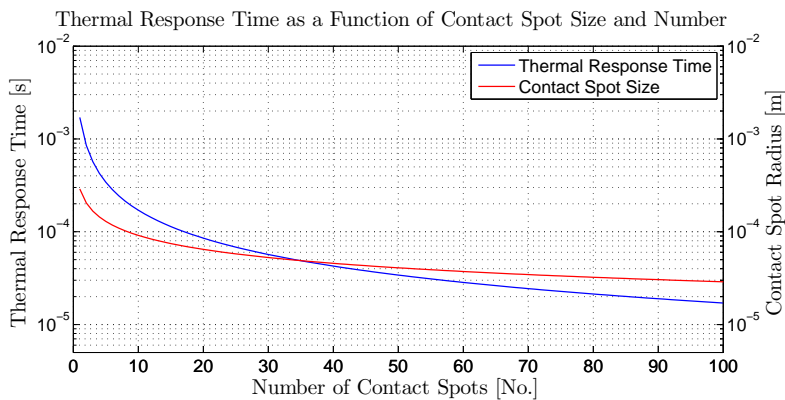


Figure 2.6: Thermal response time as a function contact spot size.

2.2 Overhead Line Connectors

The main purpose of a line connector is to both mechanically and electrically join two overhead conductors. The connection should be of such a quality that the mechanical and electrical properties of the line are not reduced because of the splice. This means that the connector must withstand both the load current and the tensile forces applied to the conductor.

2.2.1 General Description

Line connectors come in many shapes and sizes, and the complexity and shape of the construction varies depending on the type of conductor and the application of the connector. Although the construction varies, a line connector is in principle a long conducting barrel, often made out of aluminum, with a conducting cross section equal or larger than the conducting cross section of the conductor. If the conductor includes a steel core, like for steel reinforced aluminum conductors (ACSR), a separate connector is applied across the steel core to maintain the mechanical strength. The connector is applied by inserting one end of each conductor into the ends of the connector and then applying a compression pressure. Figure 2.7 illustrates a principal schematic of an ACSR line connector.

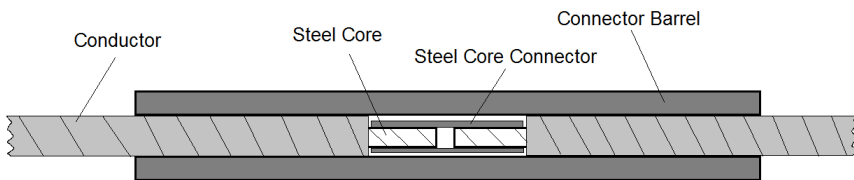


Figure 2.7: Principle schematic of an ACSR line connector.

When pressure is applied to the main connector several contact spots are created between the conductor and the connector barrel allowing the current to flow between the two conductors via the connector barrel.

2.2.2 Failure Modes

Regardless of how the connector is designed, the most common reason why line connectors fail is errors during assembly. The line should be thoroughly cleaned and any oxide layers on the conductor should be brushed off. Contaminations on the conductor may cause internal pressure during compression, thus reducing both the mechanical and electrical connection between the conductor and connector barrel. If the electrical contact becomes too poor the current starts to flow through the steel core connector causing severe heating. The connector will then lose its tensile strength and the conductor may fall down.

Installation errors may also lead to AC corrosion due to uneven current distribution, and water ingress that corrodes the steel core or creates frost bursts during

the winter. It is often a combination of all these mechanisms that causes the connector to fail [1].

2.3 Methods for Condition Assessment of Line Connectors

Today, several methods for condition assessment of line connectors are in use. These methods range from the simple and cheap like visual inspection and resistance measurements, to the more elaborate methods like x-ray inspection and thermal imaging. In this chapter the most common methods will be presented and discussed.

2.3.1 Visual Inspection

Some of the factors contributing to contact degradation may leave visual indicators. For example signs of severe heat generation is an indicator of very poor electrical contact. Frost burst may also be identified by a simple visual inspection. While this method may be performed on a live system, the best results are made when the system is offline and the component can be studied up close [1].

With the use of optical aids like borescopes, endoscopes and fiberscopes it is possible to inspect the connector in higher detail and an even more thorough visual inspection can be made. These are optical aids which transfers an image from the objective lens either by an optical relay system (Borescope or Endoscope) or a bundle optical fibers (Fiberscope).

Vattenfall in Sweden has to a large extent used borescopes in condition assessment of line connectors. By using a detector which detects changes in the magnetic field it is possible to locate the area where the steel core connector starts and aluminum conductor ends. They then drill a hole into the connector and inspect this cavity using a borescope. It is then possible to determine if the connector has started to corrode and therefore should be replaced. If the connector is fine, the cavity is filled with grease and the hole plugged. It is worth noticing that Vattenfall has had problems with some of the replenished connectors, and it is assumed that the pressure from the replenished grease has caused a contact separation [1].

2.3.2 Thermal Imaging

All objects with a temperature larger than absolute zero emits infrared waves. It is these waves an infrared camera (IR-camera) picks up and uses to determine an objects temperature. Modern IR-cameras often portray the objective as a grey-scale or blue to red-scale image where the hot part appear illuminated. This opens the possibility to fly above the overhead line and determine the surface temperature of the line connectors quickly and efficiently. This diagnostic method needs to be performed with a live system to prevent that the components from cooling down. A rule of thumb has been that the load current should be larger than half the rated current [1].

A down side to thermal imaging is that the measurements need to be corrected for external factors like radiation reflection, thermal radiation heating, load dependent heating and changes in the emission factor (soot, grease, or pollution on the connector). The reflected radiation of a component is governed by its emission factor (ϵ). Shiny metal surfaces have a very low ϵ . This means that only a small part of the measured radiation energy originate from the connector itself and that the larger part of radiation energy stem from external objects like the sun. There are also situations where the ϵ is different for the connector and the attached conductor. If the user does not take this into consideration, the object with the lowest ϵ will appear warmer than the one with the highest ϵ . Wind and rain also influence the measurements by cooling the surface temperature of the component. Therefore, to get the most accurate measurements thermal imaging should be performed during calm overcast weather, and images should be taken with equal components in the frame to provide points of reference.

The use and effectiveness of thermal imaging for condition assessment of overhead line connectors have been widely discussed. Though this method has been in use for several years few faults have been detected [1].

2.3.3 Resistance Measurements

Resistance measurements are often divided into three different types of measurements; Traditional resistance measurements or $\mu\Omega$ -measurements, resistance ratio measurements and non-linear resistance measurements. These methods are often accurate and give a good indication on the line connector's condition. The reason is that these methods measure the resistance of the contact surface, which is a more direct indicator on the connector's condition then thermal imaging and visual inspections.

Traditional Resistance Measurements

Traditional resistance measurements relies on simply measuring the resistance ($\mu\Omega$ -range) across the line connector and monitoring how it changes over time. The criteria for renewal is either a value above a certain threshold, or an increase in the resistance over time. A lot of different equipment is commercially available for measuring resistance in the $\mu\Omega$ -range.

If traditional resistance measurements are to be used to monitor the development of the line connectors condition. It is important to note that the measured resistance is both current and temperature dependent. The temperature and current that the connector is conducting should be recorded, so that the resistance value could be calculated back to a $20^{\circ}C$ -value.

Resistance Ratio Measurements

The resistance ratio (K) is a dimensionless value used as a quality measurement for current carrying equipment. The resistance ratio is the relation between the resistance of the component and a corresponding conductor length. For a line connector this means the resistance across the line connector divided by the resistance of a conductor with the same length. This relationship is illustrated in Figure 2.8.

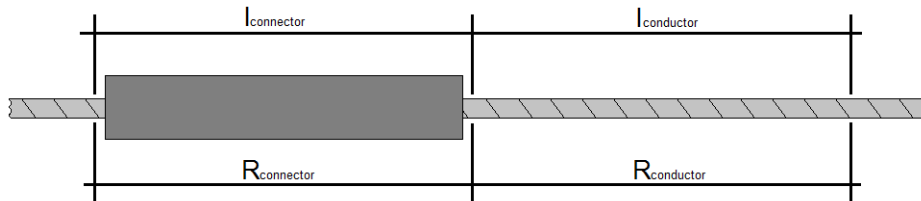


Figure 2.8: Resistance ratio measurements.

The advantage of a resistance ratio measurement is that no historical data is needed and the measurements are current and temperature independent. Typical resistance ratios are about 0.3 for a new line connector while a connector ready for replacement has a ratio of about 1.5 [1]. For a line connector the resistance ratio is defined as;

$$K = \frac{R_{connector}}{R_{conductor}} \quad (2.9)$$

2.3.4 Comparison of Resistance Measurements and Thermal Imaging

An increase in the contact surface resistance is an early indication of contact degradation and is detectable at an earlier state of degradation than a temperature increase [1]. A comparison of thermal imaging diagnostics and resistance ratio measurements has been performed by R.S Timsit [8]. The findings are presented in Table 2.1. The table shows what condition the connector was determined to be in by the two methods and what recommended maintenance actions should be performed based on the condition assessment.

Table 2.1: Recommended maintenance due to resistance ratio measurements and thermal imaging.

<i>Ratio</i>	<i>Resistance Ratio Measurements</i>		<i>Thermal Imaging</i>		
	<i>Condition</i>	<i>Action</i>	<i>Thermal Measurement</i>	<i>Condition</i>	<i>Action</i>
0.3 - 1.0	Acceptable connection	None	Connector will be cooler than conductor	Acceptable connection	None
1.01 - 1.2	Serviceable, shows deterioration	Re-inspect in one year or after next fault	Connector will be cooler than conductor	Acceptable condition	None
1.21 - 1.5	Serviceable, poor condition	Re-inspect in 6 months or after next fault	Connector will be cooler than conductor	Acceptable connection	None
1.51 - 2.0	Serviceable, very poor condition, approaching failure	Schedule replacement in less than 3 months	Connector will be cooler than conductor	Acceptable connection	None
2.01 - 3.0	Very poor condition, approaching thermal runaway	Schedule replacement very soon (days)	A slight increase in connector temperature, connector and conductor at about some temperature	Acceptable connection	None
>3.0	Thermal runaway, approaching catastrophic failure	Replace as soon as possible	Clear increase in connector temperature over conductor temperature	Deteriorating	Monitor closely

The findings show that based on the resistance measurements the degradation process is detected at a much earlier state and proper preventive actions can be performed.

2.4 Current Pulse Measurements

Current pulse measurements were earlier used by SINTEF Energy to condition assess electrical contacts inside encapsulated SF₆ equipment. This method has been adapted to apply for the condition assessment of line connectors.

As mentioned in Section 2.1.1, an electrical contact interface consists of several small contact spots. It is these contact spots that conduct the current across the interface. The contact spot resistance causes a power dissipation, which increases the contact spot temperature. The increased temperature increases the resistance of the contact spot. In reality, an electrical contact consists of several contacts spots coupled in parallel. A contact in poor condition has fewer contact spots, or the contact spots have a greater contact resistance than a connector in a good condition. Hence, if the total current is equal, the power dissipation should be greater for the poor connector.

The current pulse measurements utilizes this fact to provide a condition assessment of electrical contacts. By passing several current pulses with an increasing current amplitude, and then measuring the voltage drop across the contact for each pulse, the resistance as a function of the current can be plotted.

For a very good line connector the resistance is almost constant, while for a poor line connector the resistance has a non-linear increase with increasing current. A comparison of the resistance as a function of the current for a line connector in a very good condition and a connector in a poor condition is shown in Figure 2.9. One can see from the figure that while the resistance stays almost constant for the very good connector, the poor connector has a non-linear increase. For the poor connector alterations in the physical properties of the contact spots are also visible, indicating that melting of the contact spots have occurred. These can be seen as differences in the measured resistance for the same current.

To achieve an accurate condition assessment of a line connector using the current pulse method a current pulse source with an adjustable pulse amplitude is needed. The amplitude of the current needs to be adjusted from only a few tens amps to several times the rated current of the conductor. SINTEF Energy has achieved this is by creating a pulse source which discharges a capacitor bank through the connector. The amplitude of the current pulse is then controlled by charging the capacitor bank to different voltage levels (U_0). The pulse rise time is mainly governed by the size of the capacitor bank. In the current source created by SINTEF Energy the size of the capacitor bank is fixed, meaning that the pulse rise time is equal regardless of U_0 .

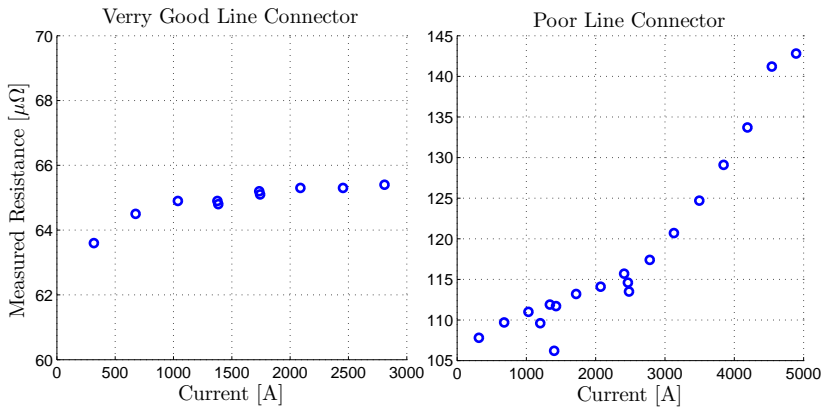


Figure 2.9: Comparison of the $R(I)$ -characteristic for a very good and poor line connector.

An electrical circuit diagram of a capacitor driven pulse source is shown in Figure 2.10. Since the resistance and inductance of the connection cables and line connector are in series they are combined into one resistance (R) and one inductance (L). The parallel capacitance between the current path and ground is assumed to be very small and therefore neglected.

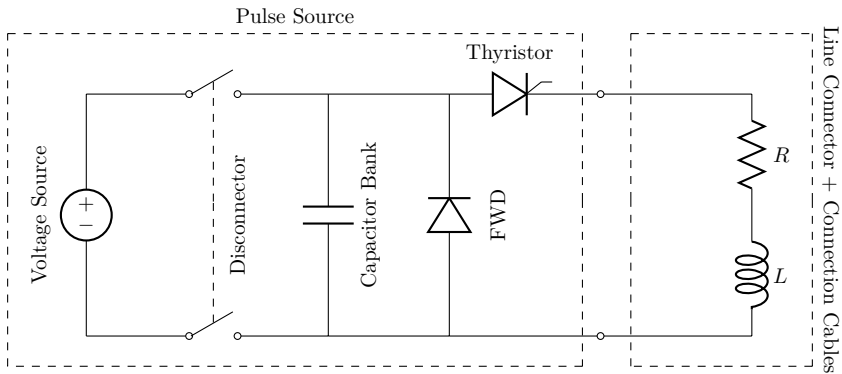


Figure 2.10: Principle schematic of the current pulse source.

The working principle of the pulse source is that initially the disconnecter is in closed position. The charging current is then allowed to flow into the capacitor bank until the bank reaches U_0 . The disconnecter is then opened to prevent any further charging of the capacitor bank. Since the thyristor is in a non-conducting state there is no current flowing through the line connector. When the system is ready to perform a measurement, a trigger signal is sent to the thyristor. This puts the thyristor in a conducting state and the capacitor bank is discharged through the line connector. A freewheeling diode (FWD) is placed in parallel with the capacitor bank to prevent reverse charging of the capacitor bank, due to the energy oscillating between L and the capacitor bank.

2.5 Mathematical Model

To understand how the different parameters of the circuit influences the current pulse, a mathematical model of the pulse source with connection cables and line connector was derived. The model was derived by removing all nonlinear elements, like the thyristor, the FWD and the voltage source, from the circuit. This strips down the circuit to a series RLC-circuit with a charged capacitor as the only source. The circuit schematic for this circuit is presented in Figure 2.11, where R is the total resistance of the circuit, including the equivalent series resistance (ESR) of the capacitor and the total inductance (L).

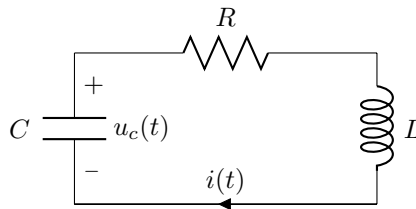


Figure 2.11: Pulse circuit model.

If the initial stored energy in the inductor is zero, the initial voltage of the capacitor becomes the governing factor. The voltage distribution and current of the circuit can therefore be expressed by the following equations:

$$u_c(t) + Ri(t) + L\frac{di}{dt} = 0 \quad (2.10)$$

$$i(t) = -C \frac{du_c}{dt} \quad (2.11)$$

By solving 2.10 with regards to u_c the expression for the capacitor voltage results in the following second order differential equation:

$$\frac{d^2 u_c}{dt^2} + \frac{R}{L} \frac{du_c}{dt} + \frac{1}{LC} u_c(t) = 0 \quad (2.12)$$

For a current pulse source the initial conditions are; $u_c(t=0) = U_0$ and $i(0) = 0$. With these initial conditions the solution to the second order differential equation (2.12) becomes:

$$u_c(t) = V_0 \sqrt{1 + \left(\frac{\alpha}{\omega_d}\right)^2} e^{-\alpha t} \cos[\omega_d t - \arctan\left(\frac{\alpha}{\omega_d}\right)] \quad (2.13)$$

By inserting (2.13) into (2.11) the current pulse created by the pulse source can be expressed by:

$$i_c = C \frac{V_0 e^{-\alpha t} (\alpha^2 + \omega_d^2) \sin(\omega_d t)}{\omega_d} \quad (2.14)$$

Where α and ω_d are the attenuation and damped natural frequency, respectively. In this case α and ω_d can be expressed by:

$$\omega_d = \sqrt{\frac{1}{LC} - \left(\frac{R}{2L}\right)^2} \quad (2.15)$$

$$\alpha = \frac{R}{2L} \quad (2.16)$$

Figure 2.12 illustrates how an estimation of the current pulse would be with $C = 390$ mF, $L = 8.0$ μ H, $R = 5.8$ m Ω , and $V_0 = 25$ V. Note that the negative current would not be possible for the actual setup since this current would flow through the FWD to avoid reverse charging of the capacitor. It is therefore the estimation of the rise time and pulse amplitude that is of importance.

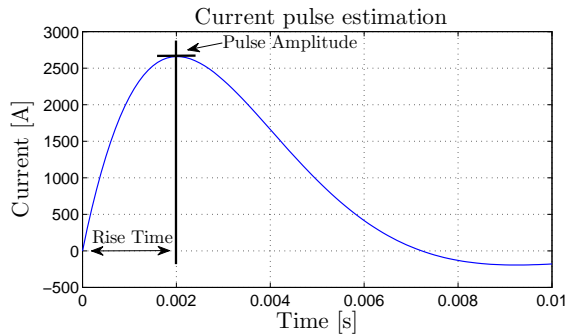


Figure 2.12: Estimation of the current pulse.

2.6 Condition Assessment Criteria

If a current passes through a contact spot the current will set up a voltage drop. Based on contact theory the magnitude of the voltage drop does not solely rely on the current magnitude but also the condition of the contact spot. A good contact spot will set up a lower voltage drop for the same current magnitude than a poor contact spot. As explained in Section 2.1.5 this voltage drop creates a temperature increase in the contact spot. Since the resistance of the contact spot is temperature dependent, and the temperature is voltage dependent, the condition of the contact can be assessed based on its $R(I)$ -characteristic. Three different states of behaviors exist [9];

1. $R(I)$ is constant. The current is sufficiently low and/or the connection is sufficiently good so that no contact spot heating occurs.
2. $R(I)$ increases with increasing current in a reversible manner. The contact spots are substantially heated and the connection is deteriorated/carries more current than it can do in a safe way.
3. $R(I)$ changes significantly and in an irreversible manner between subsequent measurements. The contact spots are so heated that local melting occurs. The connection is severely deteriorated / overstressed.

The different behavioral states are only a general description of a contact's $R(I)$ behavior and one must therefore take into account the current rating of the line when interpreting the measurements. For lines with low current ratings contact

spot heating can occur at lower current magnitudes than lines with high current ratings.

The assessment criteria used earlier by SINTEF Energy are [9];

Very good condition:

$R(I)$ is constant for current up to several times the estimated full load current

Good condition:

$R(I)$ is constant for currents up to the estimated full load current

Poor condition:

$R(I)$ increases in a reversible manner for current below the estimated full load current

Very poor condition:

$R(I)$ changes significantly and in an irreversible manner for current below the estimated full load current.

The line connectors tested in this report are also evaluated using the same criteria.

3 Prior Studies

All the work done in this project is a continuation of the student specialization project undertaken in the fall semester of 2013. The specialization project looked into how weight could be removed from the present pulse source, both by a reduction of the pulse length and a reduction in the pulse source's connection cables. This chapter is a summary of the work, results and findings from the student work; "*Condition Assessment of Line Connectors by Current Pulse Measurements - Effect of Reduced Pulse Rise Time and Connection Cable Cross Section*" [7].

3.1 Weight Reduction by Reduced Pulse Lengths

In the present pulse source the main contributor to the weight is the capacitor bank. It was earlier believed that to produce measurement with a good enough sensitivity a current pulse with a rise time resembling a 50 Hz sine wave was needed. Since the system uses electrolyte capacitors which have a relatively low energy density ¹, rise times of this magnitude require a heavy weight capacitor bank. Therefore, the main objective of the project was to look into how a reduced pulse length would affect the condition assessment.

3.1.1 Measurement Setup

To examine how the reduced pulse lengths influenced the condition assessment, assessment test with reduced pulse lengths were performed on a set of connector samples. The laboratory test consisted of two different setups. The initial setup used the already constructed pulse source with a pulse rise time resembling a 50 Hz sine wave. The condition found with these tests was meant as a point of reference, since current pulses with these lengths have been proven to provide an accurate condition assessment. The second setup was a more make shift setup that made it easy to add or remove capacitors to the capacitor bank, and allowing a larger charging voltage. All the connectors that were initially tested with the first setup was then retested using a capacitor bank of 390 mF, 20 mF, 10 mF and 2.0 mF and the condition assessment was compared with the reference test.

¹Stored Energy/Weight

3.1.2 Results and Conclusion

The results from the laboratory experiments were all conclusive, and showed that an accurate condition assessment was possible for a capacitor bank size down to at least 2.0 mF. Figure 3.1 shows the $R(I)$ -relationship for a good and a very good line connector. As described in Section 2.4, the resistance value should be almost constant for a very good line connector, while for a good connector the current should be constant below the conductors rated current. In Figure 3.1 one can see that this is true regardless of pulse length. Thus, the condition assessment would also be equal.

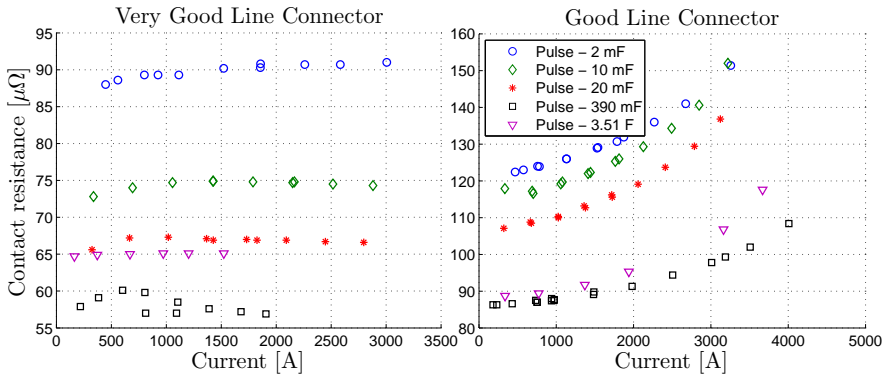


Figure 3.1: Current vs. resistance relationship with different pulse rise times for a good and very good line connector.

The measurements with shorter pulse rise times also corresponded with the reference measurements for connectors in poor conditions. Based on these findings it should be possible to drastically reduce the size of the capacitor bank, and hence the weight of the pulse source.

3.2 Reduced Connection Cable Cross Section

The second largest contributor to the weight of the pulse source are the connection cords. To reduce the total resistance of the circuit, the present pulse source utilizes connection cables with large cross sections (70 - 150 mm²) were used. It was therefore investigated, both mathematically and by laboratory tests, how the resistance of the connection cables affected the current pulse wave form.

3.2.1 Mathematical Analysis

Based on an assumption that connection cables can be seen as a cylindrical single stranded conductor, the connection cable's DC-resistance as a function of its cross section can be described by the following formula;

$$R_{Total} = \frac{\rho l}{A} \quad (3.1)$$

where ρ is the conductivity of the conductor material, and A and l is the cross section and length of the conductor, respectively.

By applying this to the circuit model presented in Section 2.5 it is possible to plot the amplitude of the current pulse as a function of the connection cable cross section. Figure 3.2 shows how the current pulse amplitude changes as a function of the connection cable cross section for different sizes of the capacitor bank. One can see from Figure 3.2 that based on the mathematical model the current amplitude should not be altered much for cross section larger than 25mm^2 . Note that this plot is based on an alteration in the systems DC- resistance.

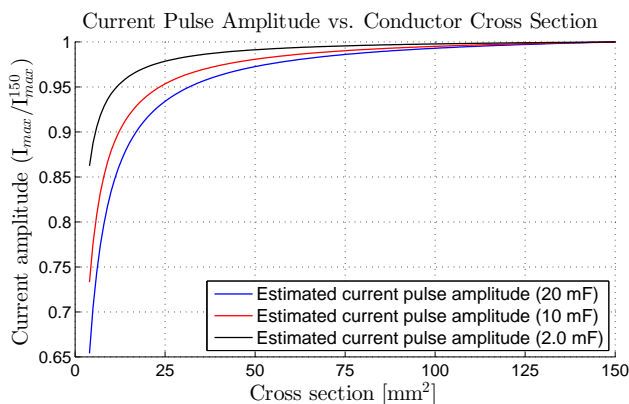


Figure 3.2: The normalized current pulse amplitude as a function of conductor cross section for different values of capacitance.

3.2.2 Laboratory Measurements

In addition to the mathematical analysis, actual measurements were performed to see how the current pulse amplitude was affected by the connection cable cross section. These tests were performed by measuring the current amplitude for three different capacitance values and for three different charging voltages for each capacitance value. The cross sections measured were 150mm^2 , 70mm^2 , 50mm^2 , 25mm^2 and 16mm^2 . The relative change in the current pulse amplitude was as expected equal regardless of charging voltage, and therefore only one charging voltage level for each capacitance value is presented in Figure 3.3. Figure 3.3 shows that the measured value corresponds well with the mathematical analysis, though the measured amplitude starts to decrease at a slightly larger cross section than the estimated. Even so the reduction in amplitude is small until approximately 50mm^2 . After this the size of the amplitude is drastically reduced.

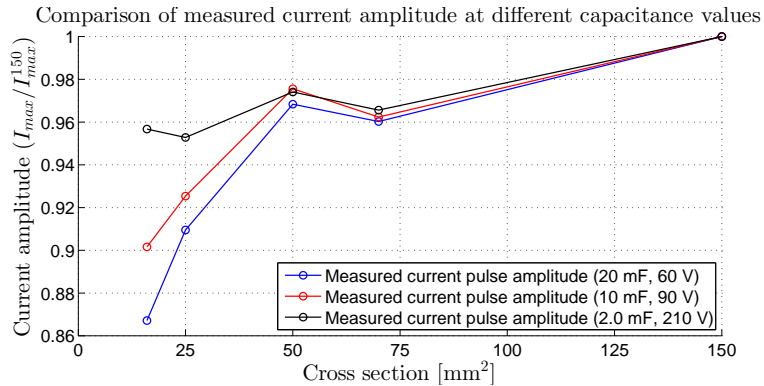


Figure 3.3: Comparison of current pulse amplitude for different values of capacitance with normalized values.

The investigations done on the effect of the connection cables cross section's influence on the current pulse wave form show that it is possible to reduce the connection cable cross section to around $25 - 50 \text{mm}^2$.

4 Current Pulse Source Prototype

One of the objectives of this report was to build a prototype of a new light weight current pulse source based on studies on weight reduction by reduced current pulse rise time and connection cable cross section [7]. This chapter presents the principle of operation for the prototype and describes each of the systems main components in detail.

4.1 Principle of Operation

As discussed in Section 3.1, prior studies show that an accurate condition assessment of line connectors using the current pulse method is possible using a significantly smaller capacitor bank. To fully utilize this, a new pulse source was built based on the following criteria;

- The pulse source should utilize a 10 mF capacitor bank, and a connection cable cross section of 35 mm².
- The pulse source should be able to run of an internal, rechargeable and portable power supply.
- The pulse source should be able to deliver a current pulse amplitude of at least 5000 A.
- To increase the flexibility of the system the sequence control should be fully programmable.

In addition to these points it was decided that the pulse source should only contain the equipment needed to adjust and produce the actual current pulse. Though it would be possible to include the equipment used for measurements and post processing, like DAQ-card, Rogowski coil, and Test Point software, these are left as separate components in the prototype.

Since the prototype should utilize a relatively small capacitor bank, but still deliver current pulses in the 5.0 kA range, the capacitor banks charging voltage needs to be substantially large. Based on (2.14), the charging voltage of the capacitor bank needs to be at least 200 V to reach such current magnitudes. A challenge related to this is that the system should also utilize a portable power supply. Portable power supplies like batteries are usually not available with such high output voltages. A solution to this could be to connect several batteries in

series to reach the desired output voltage, though this would be very impractical as the physical weight and size of the battery bank would become large. A more elegant solution would be to use a low voltage battery, and run the system through a DC/DC boost converter to amplify the voltage up to the desired level. Such converters are commercially available with many different input and output voltages, which allows an increased flexibility when deciding the output voltage of the battery. Another advantage with using a DC/DC converter is the possibility to remotely shut down the converter using a micro controller. Thus, disconnecting the capacitor bank from the battery, removing the need of a solid state relay to act as a disconnecter. A proposed solution for such a setup is presented in Figure 4.1.

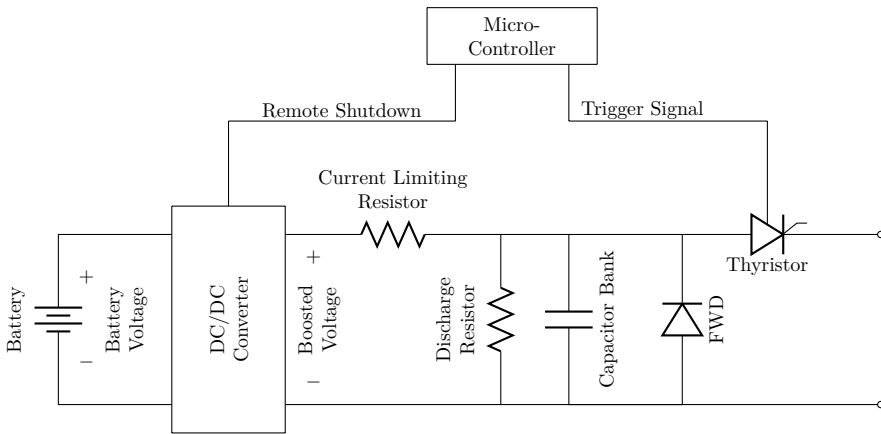


Figure 4.1: Principle schematic of circuit operation.

In the present pulse sources created by SINTEF Energy the charging voltage has been controlled either manually, meaning that the operator held a button down until the desired voltage level was reached, or by timing the duration of the charging. These methods were possible due to the size of the capacitor bank, but for the prototype these solutions would be impractical since the reduced size of the capacitor bank means that it would be fully charged in the matter of seconds. To solve this challenge it should be possible to make use of the microcontroller. By allowing the microcontroller to measure the capacitor voltage, it could remotely shut down the DC/DC converter and thereby disconnect the capacitor bank from the battery when the voltage reaches an operator specified setpoint. An illustration of the idealized charging voltage and current is presented in Figure 4.2.

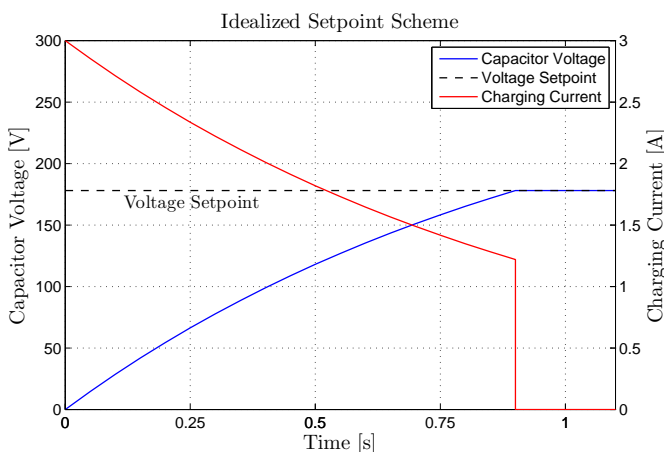


Figure 4.2: Idealized charging scheme.

Note that the voltage and current in Figure 4.2 are idealized. In reality there would be some transients when disconnecting the battery. In addition the physical delay in the voltage measurement and remote shutdown mechanism would cause the voltage to overshoot the setpoint. Therefore, to make sure that the shot is fired at the correct voltage level the microcontroller must wait until the voltage has decreased to the setpoint before sending the trigger signal to the thyristor and discharging the capacitor. To allow a faster discharge than the capacitors self-discharge, and for safety reasons, a discharge resistor is placed in parallel with the capacitor bank. Ideally the discharge resistor should have a resistance value low enough to allow a rapid discharge even at low voltages. Though high power dissipation in the resistor at high voltages limits this.

Since the charging current is greatest for low capacitor voltages the rate of which the voltage changes is also greatest at this point. This results in the voltage overshoot becoming larger for low setpoints. As mentioned the high value of the discharge resistor limits the discharge current for low charging voltages. This means that the operator needs to wait for a longer period when the setpoint is reached until the shot is fired for low voltage setpoints than for higher setpoints. To improve on this situation a current limiting resistor placed in series with the capacitor bank is added to the system. This should reduce the initial charging current and thereby the capacitor banks rate of change, thus reducing the setpoint overshoot.

4.2 User Interface

As mentioned the equipment used for measurements and post processing is placed in external components. Hence, most of the graphical representations, like results and plots, are done on an external computer. This leaves the user interface (UI) for the pulse source quite simple. Since the microcontroller is to control the entire charging and firing sequence the operator only needs to input the desired voltage setpoint. This could be done by adjusting a potentiometer which the microcontroller translates to a voltage level from 0 - 300 V. As a feedback to the user the setpoint is displayed on one of the two lines of a 16 x 2 LCD display. Such displays are available in many different shapes and sizes and are easily compatible with most microcontroller systems. The second line could be used to display the capacitor bank voltage level, or some message to the operator telling him or here that the system is ready for operation.

Besides the setpoint potentiometer, the UI needs a fire button which initiates the entire charging and firing sequence. The display could then change showing the user that the system is in charging or firing mode, before returning to the original display after the shot has been performed. Since the pulse source is still in a prototype phase it is likely to believe that the system could be used to test different microcontroller scripts. Should any of these scripts get stuck, the UI includes a reset button which restarts the entire microcontroller. To save power the system should be powered down when not in use, or between measurements. To do so a dual pole power switch is connected between the battery and the rest of the circuit. A suggestion to how such a UI might look is presented in Figure 4.3.

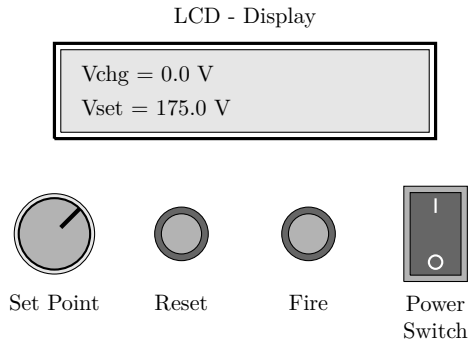


Figure 4.3: Proposed user interface.

4.3 The Prototype's Major Components

The main components of the current pulse source and why they were selected to fulfill the requirements stated in the previous section, is described and explained in the following sections. A list of the components used is presented in Appendix D.

4.3.1 Capacitor Bank

The objective of the capacitor bank is to deliver enough power and energy so that the current pulse created during discharging is sufficiently large and has an adequate duration.

As (2.14) indicates the governing factor for the pulse amplitude is the capacitance and the charging voltage. In this system the discharge current should as stated reach a maximum amplitude of at least 5000 A, while the duration and rise time is not of such importance. It is also required that the overall weight of pulse source is kept to a minimum. Since the weight of the capacitor bank follows the capacitance, it would advantageous that the capacitance of the capacitor bank is very small. Two different possibilities for the size and charging voltage is shown in Table 4.1. The maximum current peak presented in the table is based on (2.14).

Table 4.1 shows that if weight was the only criterion Alternative 1 would be the obvious choice. Also, tests from the specialization project showed that it was

Table 4.1: Values for different capacitor bank setups.

	<i>Alternative 1</i>	<i>Alternative 2</i>
<i>Capacitance</i>	2 mF	10 mF
<i>Number of capacitors</i>	2	1
<i>Maximum Voltage</i>	500 V	350 V
<i>Weight</i>	500 g	1170 g
<i>Maximum Current [Peak]</i>	5200 A	7300 A
<i>Current Pulse Rise Time</i>	0.19 ms	0.37 ms

possible to conduct accurate condition assessments with a capacitor bank as low as 2.0 mF. The disadvantage of such a low capacitance value is that it requires a large charging voltage to provide the required current pulse amplitude. Thus, the size of the capacitor bank is also determined by what maximum charging voltage that is practically possible. Since the system is to be powered by a battery, and batteries do not provide such high voltages a DC-DC converter is needed to boost the voltage to the required level. There are commercially available converters able to transform voltages from 12 V to 500 V, but such high voltages increase the contact hazard.

Even though Table 4.1 shows a substantial weight reduction between the two alternatives it was decided to use Alternative 2 for the initial prototype. This was based on the fact that a lower voltage provides a smaller operator risk, and that Alternative 2 has the possibility to provide a maximum current even higher than 5000 A. It was therefore decided to use a 10 mF aluminum electrolyte capacitor from Epcos, with a maximum voltage of 350 V. Depending on the resistance of the circuit this capacitor should be able to deliver a current pulse amplitude far above 5000 A.

4.3.2 Power Source

To power the different components of the pulse source, and to charge the capacitor bank, the system needs a power source. Since the pulse source is to be made portable, the system can not rely on power directly from the grid. The solution is therefore to apply a rechargeable battery. There are many commercially available products on the market, ranging from old fashioned lead-acid to more modern light weight alternatives as nickel-cadmium and lithium-ion batteries. In the pulse

source prototype it is important that the overall weight is kept to a minimum. Hence, a battery with high energy density would be favorable. The maximum current that the battery needs to supply is during charging of the capacitor bank. Though the initial current during capacitor charging might become quite high, this current is limited by a series resistance to about 3 A by the system. Therefore, the power density¹ does not need to be very large. An issue with many battery technologies is that they have a poor discharge profile, meaning that the battery's output voltage is reduced as the state of charge is reduced. This is necessarily not a problem for this system since the micro controller has a built in voltage regulator that regulates the controller's IO voltages. The quality of this voltage regulator is debatable and a good discharge profile would be of preference.

Based on these criteria a rechargeable lithium-ion battery would be sufficient. It has a high energy density, a flat discharge profile, and are commercially available with different energy capacities and voltage levels at a cheap price. A down side to the flat discharge profile is that it makes the battery's state of charge difficult to predict. Simple state of charge meters use the voltage level as an indicator to predict the state of charge. Since a lithium-ion battery's discharge profile shows little or no decrease in the output voltage until its capacity is almost depleted, other methods like coulomb counting must be applied to predict its state of charge.

When choosing the specifications there are two things one needs to consider; Firstly, the batteries output voltage should meet the input voltage of the other components. For this system only two components directly powered by the battery is the micro controller and the DC-DC converter. The converter is available for many different voltage inputs and the micro controller has a input voltage span from 6 - 20 V, though it favors a voltage of about 12 V. Hence, a battery output voltage of 14.4 V was chosen.

Secondly, the capacity of the battery should be sufficiently large to provide enough power for at least one entire day of condition assessing. This is a somewhat defuse criterion since the number of connectors tested in one day and the number of shots needed to assess the connector may vary greatly based on the condition of the connector. Poor connectors require more shots than a very good connector [7] [9]. An estimation is therefore made based on previous condition assessments performed in the laboratory. These tests show that a typical condition assessment requires between 10 - 20 shots. From this, and the fact that one should be able

¹*Power/Unit Weight*

to assess at least 10 connectors a day, the battery needs a capacity to deliver at least 200 shots.

Another factor counting in on the number of shots that the battery is able to deliver is the fact that not each shot has the same current amplitude. Since the charge of each shot is equal to the time integral of the current, the battery's state of charge is reduced less for shots with lower current amplitudes. Therefore, assuming that each shot is created by a fully charged capacitor is somewhat pessimistic, and it would be a better estimation to use a slightly lower value than the maximum charging voltage. The energy stored in a charged capacitor can be expressed by the following formula;

$$E_{cap.} = \frac{1}{2}CU_{cap}^2. \quad (4.1)$$

where C is the capacitor's capacitance and U_{cap} is the charging voltage. After a shot the capacitor voltage is zero, meaning that all the stored energy has been dissipated from the capacitor.

When charging the capacitor some of the energy is lost due to ohmic losses in the circuit, and also the battery's state of charge is temperature dependent. How this affects the battery capacity is not easy to predict and is therefore taken into consideration by a loss factor (ϕ).

In addition to charging the capacitor the battery should also provide power to the microcontroller and DAQ-card. The power consumption of the microcontroller is small and can be neglected in this calculation. On the other hand the DAQ-card has a maximum power consumption of 20 W, which should be running for about 4 hours. This is quite substantial and most of the batterie's capacity will be used to power this device. Thus, the energy drawn by the DAQ-card should be added to the battery's total capacity. The energy capacity of the battery needed to perform n shots can therefore be expressed by;

$$E_{batt.} = \frac{n}{\phi} \cdot E_{cap.} + E_{daq} \quad (4.2)$$

A batteries capacity is usually not expressed by the total energy, but rather by its number of amp hours. The relationship between amp hours and energy is expressed by;

$$Ah = \frac{E_{batt.}}{U_{batt.} \cdot 60^2} \quad (4.3)$$

As mentioned above the system should be able to provide at least 200 shots. The maximum charging voltage of the capacitor is 300 V, but as described it would give a more accurate calculation by using a somewhat smaller value. Therefore, when calculating the needed capacity of the capacitor bank a value of 250 V is applied. A final assumption must be made with regards to ϕ . This value represents the ohmic losses and other uncertainties regarding power loss in the system. The charging current is limited using an ohmic resistor, and it is therefore plausible to say that the ohmic losses are quite large. A value of $\phi = 0.7$ is therefore a reasonable choice.

By applying (4.1) and (4.2), and using (4.3) to convert between Joule and amp hours it is possible to calculate the batteries capacity;

$$E_{cap.} = \frac{1}{2} \cdot 10 \text{ mF} \cdot (250 \text{ V})^2 = \underline{312.5 \text{ J}}$$

$$E_{batt.} = \frac{200}{0.7} \cdot 312.5 \text{ J} + 20 \text{ W} \cdot 4 \cdot 3600 \text{ s} = \underline{377.3 \text{ kJ}}$$

$$Ah_{batt.} = \frac{377.3 \text{ kJ}}{14.4 \text{ V} \cdot 60^2} = \underline{\underline{7.3Ah}}$$

The calculation shows that based on the assumptions stated above, the pulse source battery needs a capacity of at least 7.3 Ah to produce the required amount of shots. Combining this with the need for a 14.4 output voltage, a Hy-Line Li-Ion battery with a nominal voltage of 14.4 V and a capacity of 6.75 Ah was chosen. The capacity is smaller than the calculated, but should provide enough power since the calculations are a bit pessimistic and do not take into consideration that each shot is not a fully charged shot and that the DAQ-card does not need to be powered during moving and connecting of the pulse source. The 6.75 Ah battery was therefore chosen since it has a favorable weight and size compared to a battery with a capacity larger than 7.3 Ah and a voltage output of 14.4 V.

4.3.3 Thyristor

The primary objective of the thyristor is to act as a controllable switch connecting the capacitor bank to the line connector. This means that the thyristor needs to conduct the entire current pulse. Though the magnitude of the current can become quite large the duration is very short, and this prevents heat dissipation from damaging the component. Thus, it is not necessary that the thyristor's current rating is as large as the pulse amplitude, but it still needs to be of a certain size if the thyristor is not to be damaged during operation.

Estimating this value is not straight forward. In the data sheets, the manufacturer presents a maximum RMS-value of the on state current. This is the value of the current for which the thyristor is able to continuously operate without exceeding the thermal limits. In addition to this value a 10 ms surge current value is also provided, and is often in the magnitude of ten times the continuous current rating. Even though 10 ms is a long time compared to the pulses produced by the pulse source this is the only surge current data given by the manufacturer and should be used as a design criterion.

Another factor that should be taken into consideration when choosing a thyristor for current pulse use, is the rise time of the current. A thyristor is switched on by applying a voltage between the gate and cathode. This voltage results in a carrier injection at the boundary between the n-emitter and p-base, causing only a small portion of the semiconductor interface to switch to the active state. If a sufficiently large current is applied this initial active area will spread and cover the entire available area of the device [10]. If the spreading velocity is insufficient the active area of the thyristor becomes too small to properly conduct the current, which results in an increased power dissipation. This power dissipation, if sufficiently large, may damage the thyristor. From the manufacturer this spreading velocity is defined as a maximum permissible current rise time (di/dt). As long as the current pulse rise time does not exceed this value, the spreading velocity is adequate.

An Eupec TD330N Thyristor Module fulfills the requirements stated above. In addition to a thyristor this module also contains a power diode which is able to act as the systems FWD. The maximum surge current is 8000 A, which should be sufficiently large to prevent the thyristor module from being damaged during high current pulses. Also the critical rise time (di/dt) is valued to 250 A/ μ s. Figure 4.4 shows how a curve with $di/dt = 250$ A/ μ s compares to the measured current pulse during normal operation.

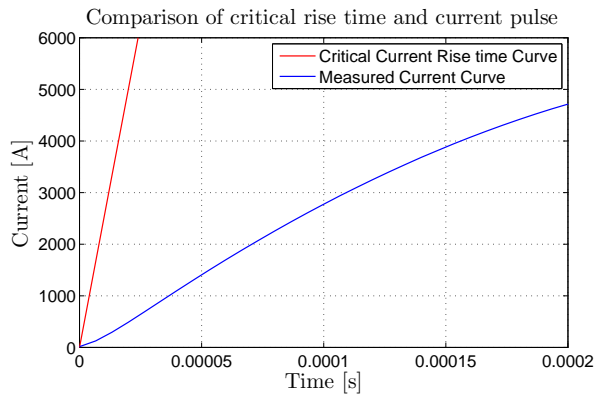


Figure 4.4: Comparison of critical rise time and measured current pulse.

As one can see from the figure, a $di/dt = 250 \text{ A}/\mu\text{s}$ is more than adequate during normal operation. In a short circuit situation the inductance of the circuit will be reduced. This will result in an even shorter current pulse rise time. It is therefore necessary to consider the current pulse rise time during short circuit instances. For this system the rise time during short circuit is unknown, but the thyristor's critical rise time should be adequate to avoid damage during short circuit instances.

4.3.4 DC-DC Converter

The nominal supply voltage from the battery is 14.4 V, and the desired charging voltage is about 300 V. To boost the battery voltage to the needed charging voltage a DC-DC converter was applied. This converter should also act as the disconnecter between the capacitor bank and battery.

Since the converter is placed in series with the battery and capacitor bank the converter has to conduct the entire charging current. For capacitor bank charging applications the initial current could become quite large, depending on the resistance of the circuit. In this system the initial current is limited by a series resistance to about 3 A. This current is only temporary and is reduced quite rapidly, and the converter's power rating does not need to be as high as the maximum charging current.

In addition, most converters are equipped with some sort of overcurrent protection scheme. This scheme either powers off the converter until a reset signal is

given, or the converter enters a "hiccup" mode which powers the converter on and off until the over current condition is gone. Since the high charging current most likely would trigger such a protection scheme the converter needs to have an overcurrent protection override to allow proper charging.

Converters designed for capacitor bank charging are commercially available with many different voltages and current ratings, and for this application a 12 V to 300 V DC-DC converter in Pico Electronic's QP-series was chosen. The reason for choosing this converter is that it has a 50 W power rating, which should be sufficient for the charging current. If this converter is to be used for capacitor bank charging applications it will not be able to start-up since the internal bias supply would not be able to provide the required start up voltage [11]. To solve this problem an external bias voltage should be applied until the capacitor bank voltage reaches 90 - 95 % of its nominal value. A control scheme of this setup is presented in Figure 4.5. While an external voltage is provided to the external bias input, the output overload and short circuit protection is disabled. It is therefore important that the external bias is disabled when the output voltage reaches its nominal value, to restore the converters protection.

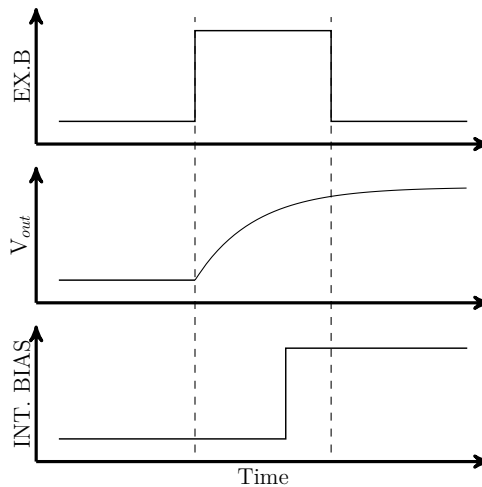


Figure 4.5: External bias (Ex.B) control scheme.

The external bias voltage is controlled by placing a reed relay between the input and external bias pin of the converter. This relay is then switched by a signal

from the microcontroller. As mentioned the capacitor bank voltage is controlled by shutting down the converter when the desired value has been reached. This is done by utilizing the remote shutdown feature of the converter. If the SHDN pin is pulled to ground the converter shuts down within $100 \mu\text{s}$.² This delay, along with the switching and microcontroller delay will result in the capacitor bank voltage overshooting its setpoint. To reduce this overshoot and still provide a galvanic insulation between the microcontroller and the system voltage a optocoupler was used to pull the SHDN pin low. A optocoupler is a component that uses light to transfer electrical signals between to signals, thus electrically insulating each side of the system. The converters pin layout and electric circuit schematic is shown in Figure 4.6. Note that the optocoupler is illustrated as a standard npn transistor in the figure.

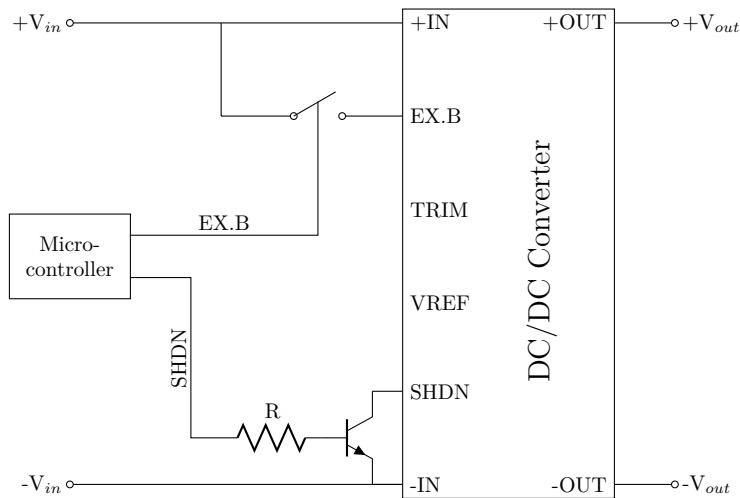


Figure 4.6: Schematic of the DC-DC converter control circuit.

4.3.5 Microcontroller Unit

To control and monitor all the different aspects of the pulse source it was decided to use a microcontroller based system. The advantage of choosing this type of system above a hardware based logics circuit is that the microcontrollers are fully

²Dennis Keleman - Pico Electronics, Email 12-02-2014

programmable. This means that the sequence control can be altered during the prototype testing to better fit the new pulse source.

The microcontroller chosen for the prototype development was the Arduino Uno. The Uno is a microcontroller, based on the ATmega328 microprocessor, with 14 digital gates that are programmed by the user to operate as an input or output, 6 analog inputs and a clock speed of 16 MHz. In addition, the Uno has a wide input voltage range (6 V - 20 V) which makes it ideal for use in battery powered applications. A circuit schematic of the Arduino Uno is shown in Appendix C and a picture of an Arduino Uno R3 is presented in Figure 4.7.

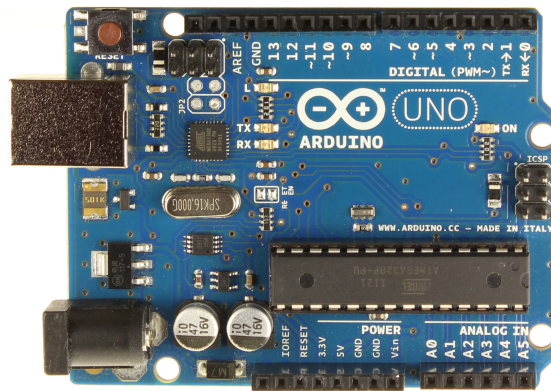


Figure 4.7: An Arduino Uno R3.

The Uno is programmed using an open source software, which compiles and transfers the code to the microprocessor via USB. The language of the code resembles the programming language C, and is compatible with all versions of Arduinos, even third party microcontrollers. In the pulse source prototype the Uno is used to measure the voltage and as a sequence controller. A downside to the Uno is that it is fairly fragile. Though the digital outputs are powerful enough to control small reed relays and transistors, short circuits or overcurrents have a tendency to destroy the output rendering it useless. Due to this a more robust solution should be chosen if a final product is to be developed. Note that "tougher" third party Arduinos exist, which utilizes the same code as the Uno.

4.4 Sequence Control

The purpose of the pulse source's sequence control is to make sure that the measurement sequence is performed in the defined and correct way. For the prototype the measurement sequence is defined as follows;

1. The system is powered up and placed in a loop state waiting for the operator to initiate the sequence.
2. When the operator pushes the fire button the sequence starts.
3. The microprocessor then reads the desired setpoint for the charging voltage.
4. If the setpoint is lower than the charging voltage a signal is sent to the DC/DC-converter removing the remote shutdown. The capacitor bank is then charged through the DC/DC-converter. If not the sequence jumps to point 6.
5. When the charging level is greater or equal to the setpoint voltage the remote shutdown is activated, terminating the charging of the capacitor bank.
6. Due to latency in the system, the capacitor bank is always overcharged. The capacitor bank is therefore slowly discharged through a power resistor.
7. When the charging voltage is less or equal to the set point a short pulse is sent to the DAQ-card to initiate the sampling.
8. After a delay of about 2 ms a triggering signal is sent to the thyristor. This short circuits the capacitor bank via the line connector and the current pulse is passed through the line connector.

A sequence diagram of the above described procedure is presented in Figure 4.8. This sequence repeats every time the fire button is pushed. Note that the sequence diagram is only an illustration and the time axis is therefore not to scale. The Arduino source code for this sequence control script is presented in Appendix B.

4.5 Sequence Control Circuits

The microcontroller is not able to trigger and control each component in the system by itself. Thus, several circuits were constructed to aid the microcontroller

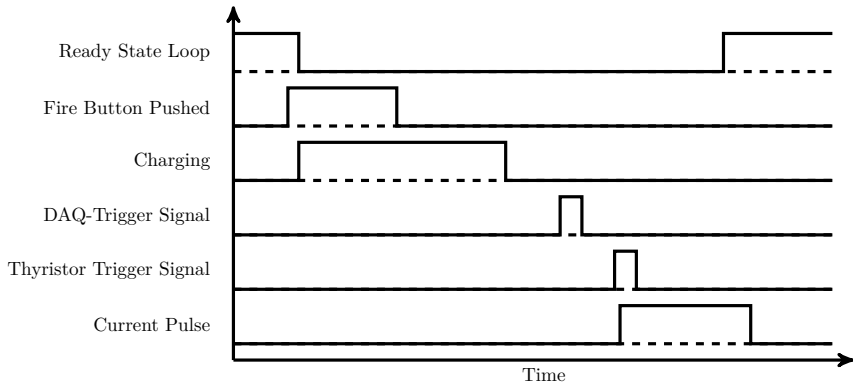


Figure 4.8: Sequence diagram for the measurement sequence.

during the different stages of the sequence control. In this chapter these circuits are presented and discussed. Both by an explanation of the working principle and by the circuit schematics.

4.5.1 Thyristor Trigger Signal

The outputs of the microcontroller is not powerful enough to trigger the thyristor by itself. Therefore, an external trigger circuit, controlled by the microcontroller, was created. The circuit schematic for the thyristor trigger circuit is presented in Figure 4.9. The circuit is activated by using the microcontroller to activate the gate on the MOSFET, which short circuits the capacitor C_1 across the pulse transformer (T_1) creating a voltage pulse. The length of the pulse is governed by the size of C_1 . T_1 has a turn ratio of 1:1 and is placed in the circuit to create a galvanic insulation between the high and low voltage side. Because the output signal voltage should not exceed 1.4 V, two diodes (D_1, D_2) are placed in series across the secondary winding of T_1 to limit the output voltage.

When the gate signal is turned off the MOSFET becomes non-conducting. To avoid a large voltage across the primary windings of T_1 due to an abrupt change in the current, D_3 is placed across the primary winding and acts as a FWD. The final two components of the circuit are the resistors R_1 and R_2 . R_1 's task is to limit the current when V_{cc} is applied to a non-charged C_1 and thereby avoiding a voltage collapse during power-up. R_2 is placed between the MOSFET gate and

ground, and acts like a pull-down resistor allowing the stored energy between the gate and ground of the MOSFET to be discharged when the gate signal is turned off, and thus placing the MOSFET in a non-conducting state.

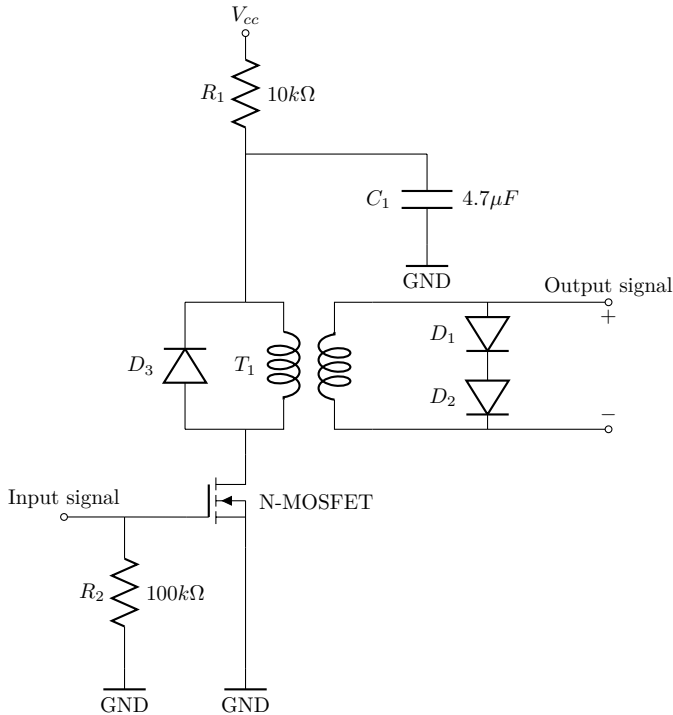


Figure 4.9: Schematic of the thyristor trigger signal circuit.

4.5.2 DAQ-card Trigger Signal

For the same reasons as for the thyristor trigger circuit, a trigger circuit for the DAQ-card was built. The working principle for the DAQ-card trigger circuit is equal to the thyristor trigger circuit, and the circuit schematics are almost identical. The only difference is that while the thyristor gate signal needs to be limited to 1.4 V, the DAQ trigger signal voltage does not need to be restricted for $V_{cc} = 14.4$ V. The diodes on the output signal gate are therefore interchanged

with a $100\text{ k}\Omega$ resistor (R_5). The circuit schematic for the DAQ-card trigger circuit is presented in Figure 4.10.

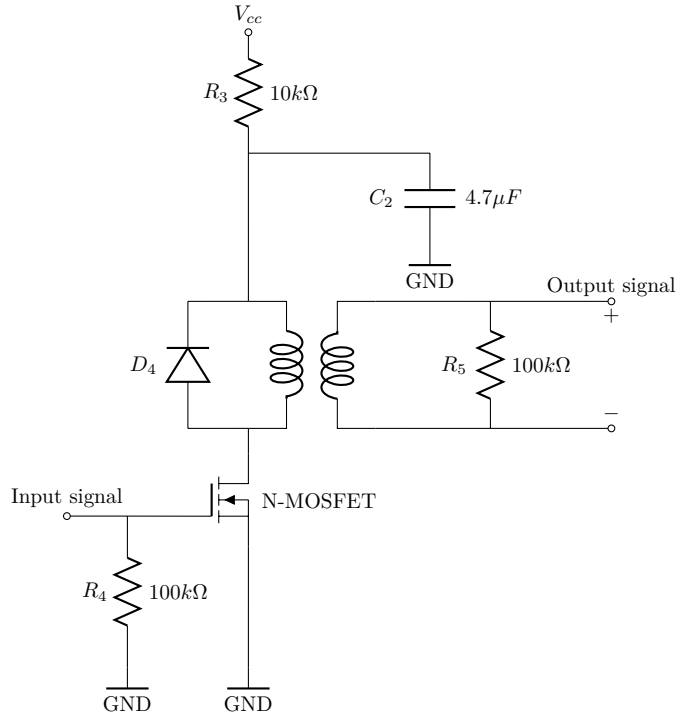


Figure 4.10: Schematic of the DAQ-card trigger signal circuit.

4.5.3 Voltage Measurement Circuit

Essential to sequence control is the microcontroller’s ability to measure the voltage. The analog inputs of the Arduino Uno only has a voltage range from 0 - 5 V. An external circuit which provides a 0 - 5 V signal that is proportional to the 0 - 300 V charging voltage is therefore necessary. To provide galvanic isolation between the high voltage and low voltage side, a measurement circuit based on the LEM LV25-P was constructed. The circuit schematics for the voltage measurement circuit is shown in Figure 4.11.

The LV25-P is a current transducer meaning that it sets up a current on the measurement gate (M) proportional to the current at the input (+HT, -HT). The highest measurement accuracy is achieved for a input current of 10 mA. This system is designed to produce this current at 300 V. Hence, a input resistance ($R_7 + R_8$) of $30\text{ k}\Omega$ was chosen. The reason for choosing two input resistances with half the total size each, was to limit the power dissipation in each resistor. With an input voltage of 10 mA the output voltage is equal 25 mA. Thus to produce a voltage signal from 0 - 5 V that is proportional to the input voltage the current must pass through a resistance of $200\ \Omega$ (R_6). The input resistance of the Arduino Uno's analog inputs are large enough that the current flowing to the measurement circuit's analog output can be neglected.

To provide an accurate input/output current relationship the LV25-P needs to be powered by a power source of $\pm 12\text{ V}$. Since the battery output is only 14.4 V, the system is not able to create the required potential difference on its own. Thus, the required potential is created from a 12 V to $\pm 12\text{ V}$ DC-DC converter (NDTD1212C).

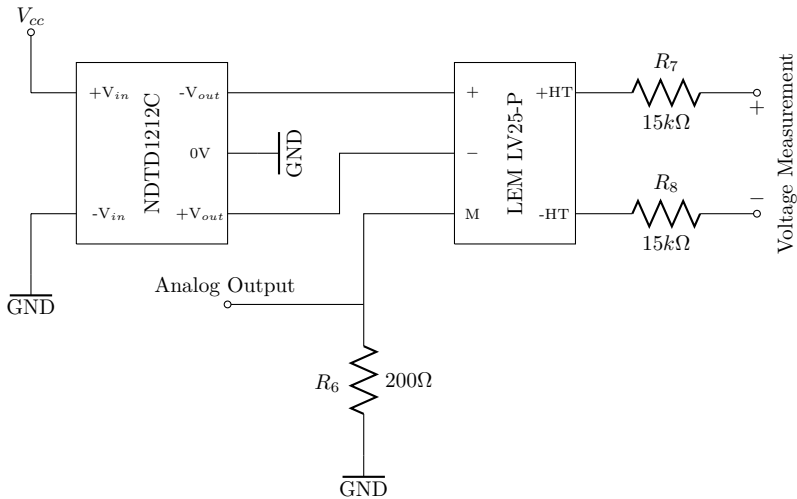


Figure 4.11: Schematic of the voltage measurement circuit.

4.6 Final Design

Since the pulse source prototype is to be used for field work it is important that the components are protected against external hazards like dust and water. Thus, for the final design of the prototype, it was decided to place all the components inside a Pelican 1450 Case. This is a high performance case which provides a watertight and dust proof environment for the components, while keeping a compact and portable design. All the components were then attached and securely fastened to an aluminum plate, which was secured to the Pelican case. This was done to avoid puncturing the case and therefore maintaining a relatively watertight design. Note that the aluminum plate is punctured to fasten the components and for cable feedthroughs and it is possible that these locations could lead to water ingress.

To ease the access to the microcontroller, DAQ and thyristor trigger signal circuits, and the voltage measurements circuit, these components were placed on top of the aluminum plate. To protect these components while the lid of the Pelican case is open, the components are placed underneath an internal aluminum case. This internal case is equipped with a BNC-connector to allow a trigger signal to be sent to the DAQ-card.

The UI of the prototype is placed on the top half of the aluminum plate and consists of an 16x2 LCD Display, a power switch, a fire button, a reset button, and a setpoint potentiometer. In addition to what was discussed in Section 4.2, the user interface includes one 2.1/5.5mm DC jack outlet for powering the DAQ-card, and a 2.5/5.5mm DC jack inlet for battery charging. All the components of the user interface is labeled accordingly.

A new system for attaching the connection cables was also derived. While the old system used a simple nut and bolt principle the prototype applies a power connector. The female connector is placed on the aluminum panel and the male contact is placed on the connection cords. This increases the user protection compared to the old system significantly, since the female connector has an IP code of 20, meaning that no solid particle larger than 12.5 mm can come into contact with conducting parts. This system is also more time efficient when setting up or taking down the measurements as it is simply a plug and play system. A picture of the prototype's final design is presented in Figure 4.12.

Since the overall objective of this project was to design and construct a portable and light weight pulse source prototype, the physical properties of the final design



Figure 4.12: Picture of the prototype's final design.

is also of great importance. Thus, measurements of the external dimensions and weight was conducted. The physical properties of both the old pulse source and the prototype pulse source are presented in Table 4.2. The values presented in the table only includes the weight of the pulse source itself and does not include the weight of any external components like connection cords or DAQ-cards.

Table 4.2: The pulse source prototype's physical properties.

<i>Physical Properties</i>	
<i>L x W x D [cm]</i>	<i>Weight</i>
<i>Pulse Source Prototype:</i> 40.6 x 33 x 17.4	7.6 kg
<i>Old Pulse Source:</i> 52.5 x 49 x 27.5	36 kg

As seen from Table 4.2 the pulse source prototype is more compact and weighs considerably less than the previous pulse source.

5 Condition Assessment Tests

To prove the validity of the pulse source prototype the equipment was tested on several line connectors removed from different power grids. These line connectors, the test methods, and results from the laboratory tests are presented and discussed in the following sections.

5.1 Connector Samples

As a proof of concept, the pulse source prototype was used to condition assess three line connectors with a previously know condition, and ten line connectors with an unknown condition. These samples all have in common that they have been removed from actual power grids, where they have been naturally degraded. All samples contain a line connector with a small piece of conductor attached to each side (1 - 2 m).

5.1.1 The French Connectors

The line connectors with a know condition were a part of a set of line connectors previously tested by SINTEF. These line connectors and the results from the previous condition assessment is presented in detail in the project memo "*Line Joints Removed from The French Grid*" [9], and will from here on out be referred to as the French Connectors.

In "*Line Joints Removed from The French Grid*" several line connectors were tested. In the project memo these connectors were each labeled with a number from 1 to 13. This report will use this number when referring to one of the French Connectors. For the retesting using the prototype pulse source only three of the French Connectors were selected. As their condition was already known, they were selected based on their condition. Hence, one very good, one good, and one poor connector were chosen for retesting. Thus, the line connectors selected were nr. 1, 6 and 11. The type and condition of the conductor connected to these line connectors vary, and so does the connector type. Hence, a more thorough description of the selected connectors is presented in Appendix A. -

5.1.2 The Finnish Connectors

In addition to the French Connectors ten other connectors were provided by Fingrid. These connectors were removed as a part of a planned renewal and capacity upgrade of an old power line in Finland, and not based on any form of condition assessment.¹ Hence, the condition of these connectors are totally unknown. From here on out these connectors will be referred to as the Finnish Connectors. A picture of one of the Finnish Connectors is presented in Figure 5.1



Figure 5.1: A picture of one of the Finnish Connectors.

For the Finish Connectors all ten samples were chosen for testing. The connectors were all removed from the same line, thus the attached conductors are all of the same type. The code name for this particular conductor type is Ostrich.² The technical data of an Ostrich conductor is presented in Table 5.1. The connectors have all been compressed using hydraulic pressure.¹

Table 5.1: Technical data for an Ostrich conductor.

Code Name	Areas			No. of wires		Wire Diameter		Diameter		DC Resistance Ω/km
	mm^2	mm^2	mm^2	Al	Steel	mm	mm	mm	mm	
	Al	Steel	Total	Al	Steel	Al	Steel	Core	Cond	
Ostrich	152.2	24.7	176.9	26	7	2.73	2.12	6.36	17.28	0.1898

Based on the information presented in Table 5.1, it is possible to estimate the conductors rated current. For an Ostrich conductor the rated current at $75\text{ }^\circ\text{C}$ is found to be 492 A. A table presenting the technical data with current ratings for several different types of conductors is presented in Appendix E.

Though the connector and conductor of the Finish Connectors are equal, the external physical condition varies somewhat. Non of the connectors seem to have

¹Mikko Jalonen - Fingrid, Email 26-04-2014

²Svein Magne Hellesø - Sintef Energy, Email 24-4-2014

any visual external corrosion, but several of the connectors have been exposed to some kind of pollution, and are therefore quite darkened in color, and have a dirty surface.

The Finnish Connectors were all delivered without any individual labeling. To provide a system of reference, the connectors were numbered from one to ten defined by the measurement order. To distinguish the Finnish from the French connectors, the reference system places the word FIN in front of the number when referring to one of the Finnish Connectors. Thus, connector number 6 of the Finnish Connectors is referred to as FIN06. In addition, it must be possible to distinguish between the different sides of the connectors. A label with the name of the connector is attached to one of the sides of the connector. In this report this side is referred to as "Side A". An illustration showing the reference system for the Finnish Connectors is presented in Figure 5.2.

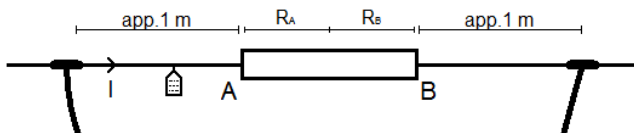


Figure 5.2: An illustration of reference system used on the Finnish Connectors.

5.2 Methods

When condition assessing the French and Finnish connectors a specific measurement procedure was followed. This procedure including the equipment used, and a description of the measurement setup are presented in the following sections.

The connector samples are assessed using the condition criteria presented in Section 2.6.

5.2.1 Equipment

Besides the pulse source prototype and the line connector samples, the equipment used in these measurements is;

- Computer with Test Point software able to capture and process the measurements (Panasonic Toughbook) (P07-1320)
- DAQ Card with two inputs, and external trigger (National Instruments USB-6251 M) (G05-0153)
- Analog low-pass filter (ω_k) (SINTEF Energy)
- Rogowski coil with current transducer ($I_{max} = 6000$ A) (PEM CWT-30R) (I04-0421)
- Two RK 25mm² connection cables
- One braided copper wire (35 cm) with cable connections and rubber band
- One specially designed connection clamp (SINTEF Energy)
- Coaxial Cables
- Assorted connection equipment

5.2.2 Measurement Setup

The measurements were all carried out with the connectors lying on the laboratory floor. To be able to condition assess each side of the connectors individually the voltage meter was connected as shown in Figure 5.3, and switched over to the opposite side after the first side was assessed. Note that since the current is passed through the entire line connector the contact spots on the opposite sides may be influenced by the current. Figure 5.3 shows how the measurements were set up.

The connection cords from the pulse source is connected to the excess conductor using the braided copper wire and rubber band on one side, and a specially designed connection clap on the other. Both the braided wire with rubber band, and connection clamp have been proven to give a good connection to the excess conductor without damaging it [12]. The reason for using two different methods to connect the pulse source to the line connector was that only one connection clamp was available during the time of testing.

The current is measured using a rogowski coil, but since a rogowski coil actually measures the time derivative of the current, an integration of the signal is required. This is done by a current transducer before feeding the signal into the

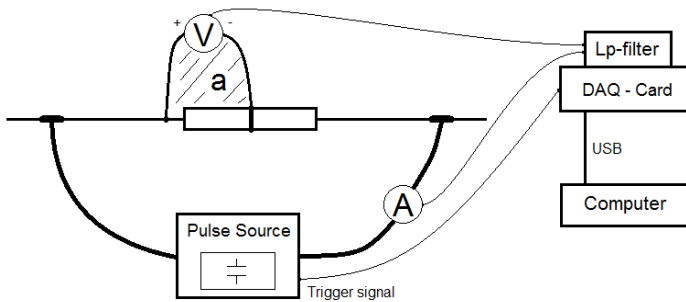


Figure 5.3: Measurement setup for the prototype condition assessment tests.

DAQ-card via the low-pass filter. The voltage is measured directly by the DAQ-card. To reduce the measurement error caused by induced potential differences in the voltage measurement loop the connection cords of the voltage measurement should be intertwined to reduce the loop area. This area is illustrated as the area "a" in Figure 5.3.

5.2.3 Measurement Procedure

The condition assessment measurements performed in these test follow a specific measurement procedure. Prior to the current pulse measurements, the DC-resistance for each side of the connector is measured. This is not done solely to determine the DC-resistance, but also to determine which side of the line connector should be measured first. The reason for doing so is that this measurement setup causes the current to pass through both contact interfaces of the connector, while only measuring the voltage drop across one interface. Since the interface with the highest DC-resistance should be the one to produce the largest voltage drop, alterations in the contact resistance caused by melting or softening of the contact spots should occur at a lower current than the side with the lowest DC-resistance. Thus, it should be possible to perform current pulse measurements on one side without causing alterations on the opposite.

Figure 5.4 show a flow chart of how the current pulse measurements were performed. In the chart I_n refers to the rated current of the conductor, while \hat{I}_p refers to the peak value of the current pulse. The condition where $\hat{I}_p \gg I_n$ is used in the flow chart as an "end of measurements"-criterion. This is a quite relative value, and must be defined by the user. If the purpose of the measurement is to

find the melting point of even the good and very good connectors, then this limit should be pushed much further than if only a condition assessment is required. In this report the conductors were subjected to quite high currents and the measurements on the good and very good connectors did not end until $\hat{I}_p \approx 10 \cdot I_n$, which is far above what is needed to condition assess the line connectors.

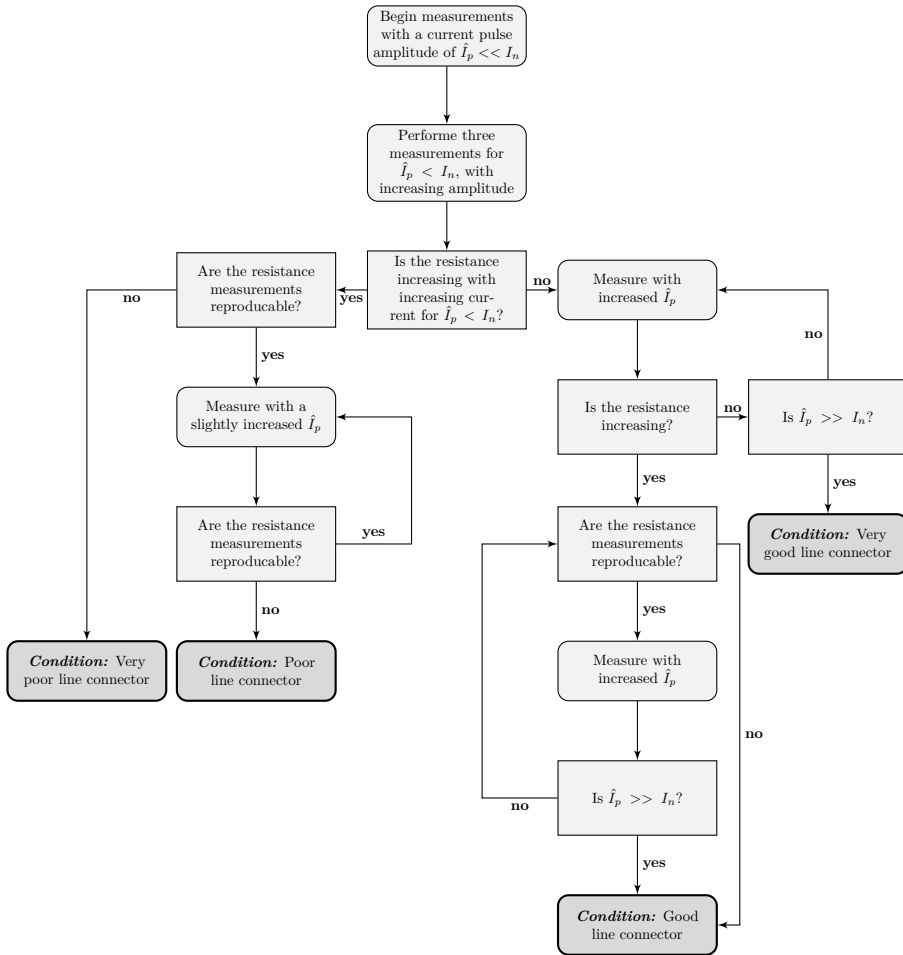


Figure 5.4: Measurement procedure flow chart.

5.3 Results and Discussion

The tests and measurements were divided into two sections. First the selected French Connectors were tested to prove the validity of the new pulse source. Afterwards the Finnish Connectors were tested using the same equipment, to look into how pulse source prototype handles during an actual condition assessment. All the measurements were performed with the setup and procedure presented in the two previous sections. Since many of the findings are equal only the major findings are presented and discussed in this report. The rest of the measurements are presented and discussed in Appendix A.

5.3.1 The French Connectors

As presented in 3.1, prior studies show that an accurate condition assessment is possible with even lower rise times than the ones produced by a 10 mF capacitor bank. To validate the new pulse source prototype the results from the prototype measurements were compared with prior condition assessment tests on the same connectors [7][9]. Since the prototype utilizes a 10 mF capacitor bank, the results are compared with measurements performed with the same pulse lengths (10 mF). In addition, the results are also compared with results found using a 3.51 F capacitor bank, which produces pulses with rise times resembling a 50 Hz sine wave. The longest pulses are referred to as the reference pulse. The results are presented based on the condition of the line connector.

Very Good Connectors

Based on the condition assessment criteria described in Section 2.6 and contact theory, a very good line connector should show very little or no increase in the resistance with increasing current for the entire current range. From the condition assessment test using the prototype pulse source the longer conductor side of the Connector 1 was found to be in this condition. A comparison of the different measurements performed on Connector 1 is shown in Figure 5.5. As Figure 5.5 shows, the three different measurements all conclude with a connector in a very good condition.

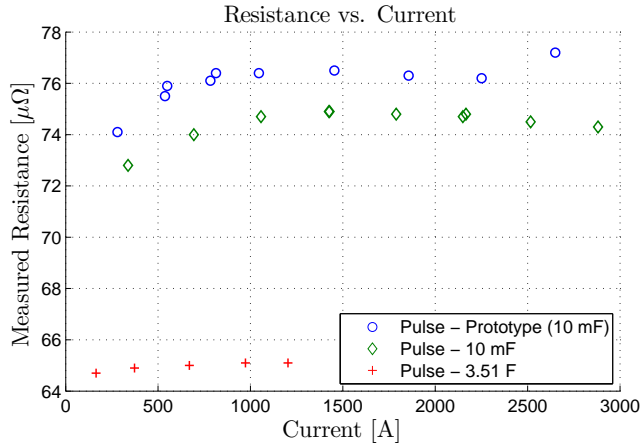


Figure 5.5: Longer conductor side of Connector 1.

There are two things worth noticing with these measurements. Firstly, the increase in resistance with increasing current at low current magnitudes. As seen from Figure 5.5, the resistance increases with increasing current up to about 1000 A before stabilizing. This seems to be present in all prior measurements as well, but the increase is greater for pulses with shorter rise times. Since the measured resistance is constant for high currents it is likely to believe that this is caused by low measurement accuracy at small currents for the rogowski coil. This phenomenon should be studied closer as it might result in condition assessment errors. Secondly, the prototype pulse source gives an overall higher resistance for the same current magnitude than the prior 10 mF measurements. Since both sources utilize a 10 mF capacitor bank, the pulse produced should be almost identical given that the inductance of external circuit is equal. Thus, the penetration depth of the current should be equal for both measurements and the overall resistance should therefore be equal. An explanation to this might be that the external circuit has changed, and the prototype therefore produces a steeper current pulse. Both these observations will be looked closer into in Section 5.4 and 5.5.

The shorter conductor side of Connector 1 and the longer conductor side of Connector 6 was also found to be in a very good condition. This correlates with the previous measurements. The above mentioned anomalies are also present in these measurements.

Good Connectors

For a connector in good condition the resistance should be constant for currents inside the area of the conductors rated current. For the French Connectors the rated current is not known, but it is possible to make an estimation based on the physical properties of the conductor. The longer conductor side of Connector 11 shows only a small increase in the resistance up to about 750 A. Based on the physical properties of the conductor this is above the estimated rated current of the conductor. For higher currents the resistance starts to increase in a reversible manner. The prototype measurements therefore conclude that the longer conductor side of connector 11 is in a good condition. As seen in Figure 5.6 this correlates with the previous measurements.

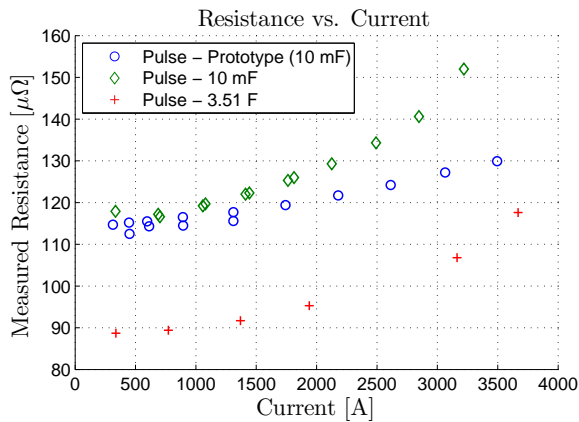


Figure 5.6: Longer conductor side of Connector 11.

While the measurements presented in Figure 5.5 show an increase in the overall resistance for the measurements performed by the prototype pulses compared to the prior 10 mF pulses. The measurements of the longer conductor side of Connector 11 shows an almost identical value in the resistance. In fact, for large currents the resistance is lower for the prototype measurements than for the 10 mF source. As mentioned this could be caused by an alteration in the circuit's total inductance, which has altered the shape of the current pulse. A comparison of the pulse rise times followed by a discussion is presented in Section 5.4.

Poor Connectors

For a connector to be assessed as poor, the resistance must show an increase in a reversible manner for currents lower and equal to the nominal load current. For the French Connectors the only connector showing this pattern is the shorter conductor side of Connector 6. A comparison of the different measurement results for shorter conductor side of Connector 6 is shown in Figure 5.7. The figure shows that the measurements performed with the pulse source prototype correlate with the previous measurements.

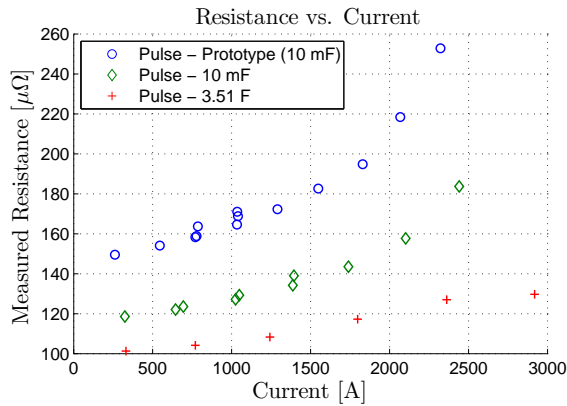


Figure 5.7: Shorter conductor side of Connector 6.

It is important to note that if the measurement error at low currents present in Figure 5.5 also is present in Figure 5.7, this would alter the connectors $R(I)$ -characteristic. Thus, providing a faulty condition assessment. In the test performed by SINTEF Energy [9], the condition for the shorter conductor side of Connector 6 was found to be in a good condition. This might indicate that a measurement error at low currents has influenced the $R(I)$ -characteristic shown in Figure 5.7.

Very Poor Connectors

No connector samples in a very poor condition were available. It is not expected that any of the above mentioned anomalies would influence the assessment of such a connector, since connectors in a very poor condition show a distinct $R(I)$ -relationship.

5.3.2 The Finnish Connectors

As mentioned, a set of ten connector samples were provided by Fingrid. For these connectors no prior measurements exist and the condition of the connectors is therefore unknown. Thus, the reasons for these measurements were to see how the pulse source prototype operates, and to further study observations made during the measurements on the French Connectors.

All the ten connector samples were condition assessed using the pulse source prototype. The connectors were all tested on both sides, which for the Finnish Connectors are referred to as Side A and B. The results and conclusion of the condition assessment are presented and commented in Appendix A. Note that the connectors have been subjected to currents far above the rated current of the conductor (492 A), and the condition assessment has thus been quite harsh.

The measurements showed that the operation and use of the prototype during condition assessment worked as intended, though the increase in measured resistance at low current magnitudes was also present in these measurements. In addition a few alterations were made to the final design to improve upon the functionality of the prototype. These alterations are described in detail in Section 6.3.

5.4 Increased Pulse Rise Time

In section 5.3.1, it was shown that the pulse source prototype almost consequently produces a slightly larger resistance value for the same current compared with the previous 10 mF measurements. It was believed that this could be due to an alteration in the circuit, which has reduced the total inductance and thus reduced the current pulse rise time. From the measurements of the French Connectors almost all of the pulses produced by the prototype show a lower rise time compared to the 10 mF measurements performed earlier. A comparison of current pulse produced with the prototype and the previous 10 mF pulse is shown in Figure 5.8.

This reduced rise time could explain why the measured resistance becomes larger when using the prototype compared to the previous 10 mF measurements, but there are a couple of deviations. Figure 5.6 shows a comparison of the measured resistance for Line Connector 11. In this Figure the measured resistance from the prototype measurements are lower than the 10 mF measurements. If

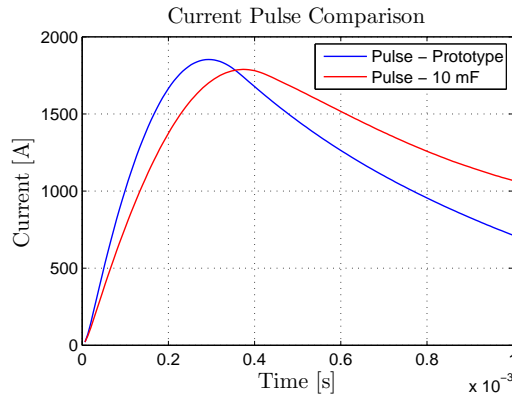
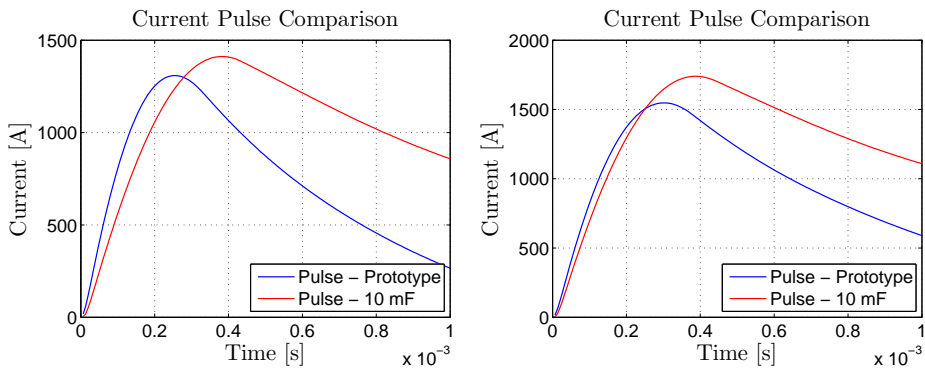


Figure 5.8: Comparison of the current pulse produced by the pulse source prototype and the previous 10 mF pulse.

the difference in measured resistance is caused by a difference in the rise time alone, the rise time of current pulse in these two measurements should be almost identical. A comparison of the current pulses used to measure the longer side of Line Connector 11 is presented in Figure 5.9a. The figure shows that the rise time is not identical for the two pulses as expected from the comparison of the measured resistance. The shorter side of Line Connector 6 also deviates from what is expected from the resistance measurement comparison shown in Figure 5.7. The figure shows an increase in the measured resistance compared to the 10 mF pulse. In Figure 5.9b a comparison of the current pulse is presented, which shows that the rise time of the current pulses are almost identical.

Based on these findings it is clear that the increase in the measured resistance is not solely caused by an reduction in the rise time, and that it is possible that other variables in the measurements have caused the increase seen in the measured resistance. Differences in the ambient temperature for the two measurements could cause differences in the connectors bulk resistance, thus increasing the measured resistance.



- (a) Comparison of the current pulse produced by the pulse source prototype and the previous 10 mF pulse for the longer side of Line Connector 11.
- (b) Comparison of the current pulse produced by the pulse source prototype and the previous 10 mF pulse for the shorter side of Line Connector 6.

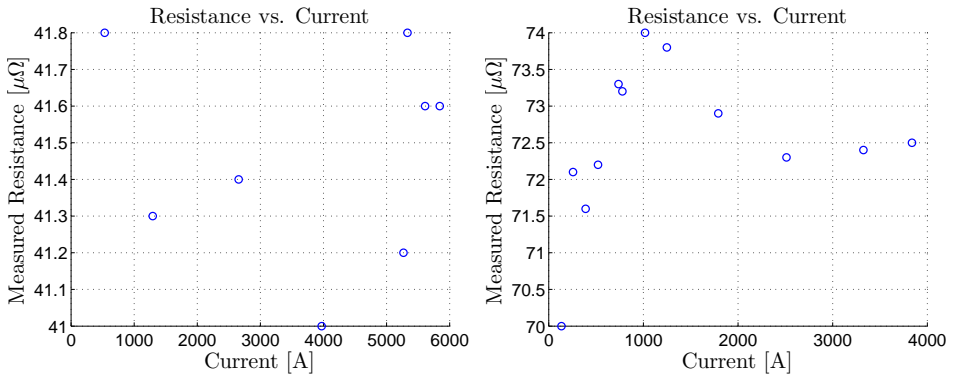
Figure 5.9: Current pulse comparison for the longer side of Connector 11 and the shorter side of Connector 6.

5.5 Resistance Increase Error at Low Current Magnitudes

During the condition assessment test on both the French and Finnish Connectors it was observed that the $R(I)$ -characteristic showed an increase in the resistance with increasing current at low current magnitudes. Since this observation could potentially cause faulty condition assessment, it is important to further study this phenomena.

Since all the measurements are done using the same measurement equipment it would be expected that resistance versus current plot of all connectors in a very good condition would show this increase in resistance. A comparison of the measurements performed on two different connectors who were both found to be in a very good condition is presented in Figure 5.10. While Figure 5.10b shows a distinct increase in the resistance at low current magnitudes. Figure 5.10a does not show the characteristic increase in the resistance. The measurement plot for side B of FIN01 differs from almost every other resistance versus current plot because it contains only one measurement below 1000 A, and this might be the

reason why the resistance increase is not present in Figure 5.10a.



(a) Measurement plot of connectors in a very good condition without increase in the resistance at low currents (FIN01 - Side B). (b) Measurement plot of connectors in a very good condition increase in the resistance at low currents (FIN06 - Side A).

Figure 5.10: $R(I)$ -plot of connectors in a very good condition with and without increase in the resistance at low currents.

In addition, the measurements show that the increase in resistance is not constant in size, but consequently ends at about 1000 - 1500 A. An example of this is presented in Figure 5.11. While the resistance for side A of FIN03 only increases with $1.0 \mu\Omega$, side B of FIN03 increases with $3.0 \mu\Omega$ within the same current range. The fact that resistance increase is within the same current range for all connectors further increases the belief that this is caused by the measurement error at low currents. Since the resistance value is almost equal for both side A and B, it is not solely the difference in voltage drop that causes the difference in increased resistance.

As mentioned, since all the measurements use the same equipment, it is likely to believe that the resistance increase at low currents is present for all measurements, also for connectors in poor condition. Since the condition criteria for a poor connector is a reversible increase in the resistance for low current magnitudes, the resistance increase caused by measurement error might cause a faulty assessment. Especially if the resistance increase caused by measurement error overlaps the resistance increase caused by poor contact spots.

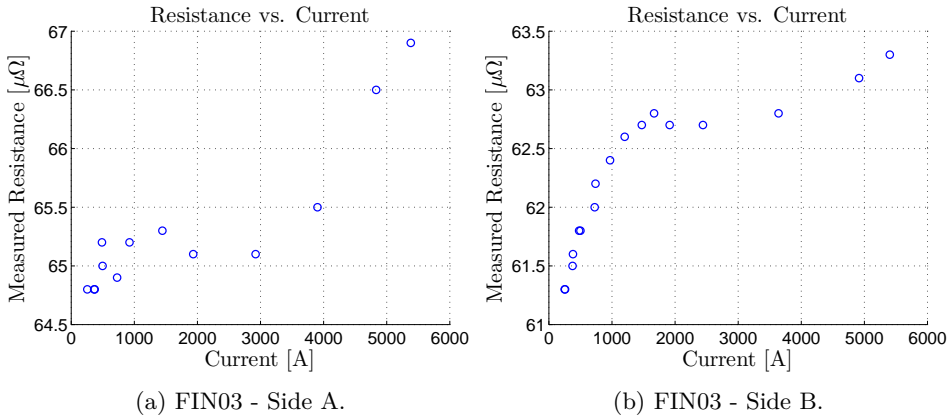


Figure 5.11: $R(I)$ -plot of connectors in a very good condition showing the difference in increased resistance at low current magnitudes.

Both sides of FIN10 was found to be in a poor condition. Figure 5.12 shows the measurement plot for side B of FIN10. The plot has been modified slightly by removing the subsequent measurements at the same current magnitudes. This is done to easier see how the resistance changes with increasing current (Figure 5.12a). In addition a zoomed plot with reduced x- and y-axis is presented in Figure 5.12b. The plots show a small decline in the curve at around 400 A, but it is not possible to tell if this is caused by an overlap of the measurement error and poor contact spots. It is therefore important that this problem is looked further into for connectors in a very good condition, where the resistance increase is prominent. If the problem is removed for those connectors it is likely removed for the poor connectors as well.

One explanation to the increase in resistance with increasing current at low current magnitudes could be that the equipment used to measure current has a measurement error at low current magnitudes. The rogowski coil used during the measurements has a maximum current rating of 6000 A. Though, in theory a rogowski coil should have a good linearity, it is possible that it becomes inaccurate for currents below 1000 A. Thus, to look into how the rogowski coil influences the measurements at low currents, side A of FIN07 was retested using a Fluke i2000Flex rogowski coil (I04-0357). This particular rogowski coil has a maximum current rating of 2000 A, and should therefore have a better accuracy for currents

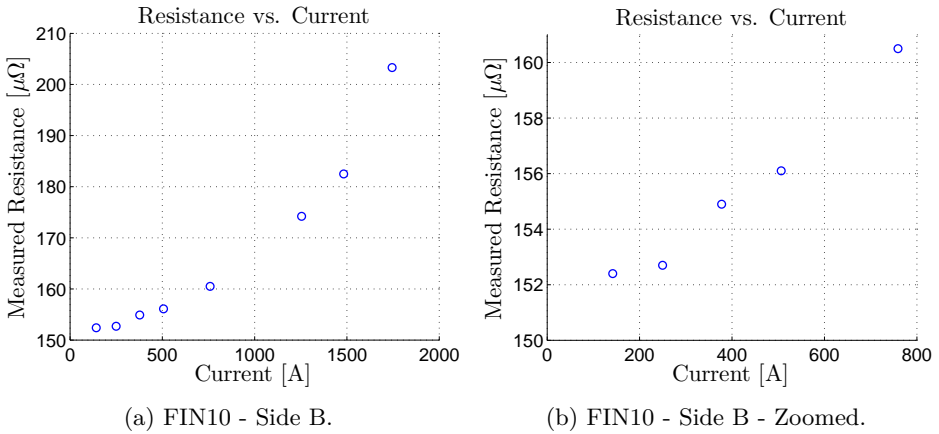


Figure 5.12: Modified measurement plot for side B of FIN10.

below 1000 A. It also has the same voltage per current ratio (1 mV/A) as the previous rogowski coil, meaning that it fits right into the system without any modifications to the post processing software.

In addition to the new rogowski coil, measurements were made using a hall effect transducer (I04-0088) with a nominal current rating of 500 A RMS, and with the same rogowski coil as for the previous measurements, but with the one of the connection cables passed twice through the coil loop. Passing the current through the coil loop twice doubles the measured current. Thus, increasing the sensitivity of the rogowski coil. Note that when doing so the post processing software needs to use only half the current when calculating the resistance.

The reason for choosing side A of FIN07 was that this connector shows a distinct increase in the measured resistance at low current magnitudes. The connector was also found to be in a very good condition, meaning that based on contact theory, no increase in the measured resistance should be present.

The measurements were performed by passing several current pulses through the connector while increasing the current for each shot. Like for a typical condition assessment test, the current and measured resistance was recorded for each shot. The plot from each of the different measurement methods is presented in Figure 5.13.

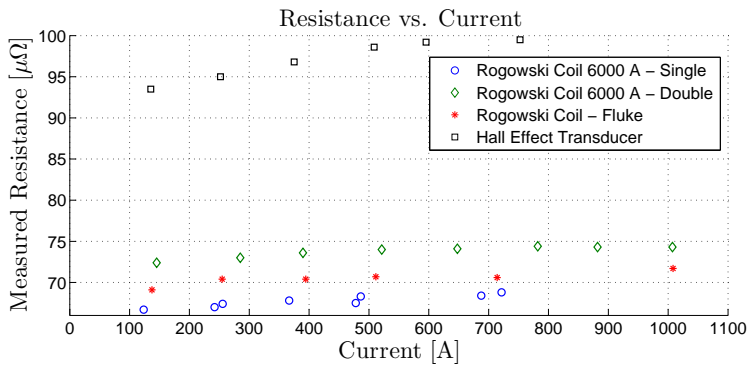


Figure 5.13: Comparison of the increase in measured resistance with increasing current at low current magnitudes for different measurement techniques.

From the figure one can see that regardless of how the current is measured, the measured resistance increases with increasing current at low current magnitudes. What is interesting to note is that while the measurements using a rogowski coil give results where the measured resistance only deviates with 2-5 $\mu\Omega$ from each other, the hall effect transducer shows a measured resistance almost 20 $\mu\Omega$ higher. The measurements made with the hall effect transducer also show a larger increase in the measured resistance with increasing current.

These observations indicate that the measurement error at low current magnitude is not located in the actual measurement equipment.

6 Prototype Functionality Tests

The functionality tests were set up to directly look into aspects of the prototype design that was not defined during the condition assessment tests. The functionalities tested were the battery lifetime and setpoint accuracy of the prototype.

6.1 Battery Lifetime

The prototype should be designed with an adequate battery capacity, though as mentioned in Section 4.3.2, a Lithium-Ion battery's state of charge is hard to determine. Hence, the battery lifetime test was conducted to try and evaluate the prototype's battery capacity.

6.1.1 Equipment and Measurement Setup

In addition to the pulse source prototype with connection cables, the equipment needed for this test was;

- Digital Multimeter (S03-0421)
- DAQ Card with two inputs, and external trigger (National Instruments USB-6251 M) (G05-0153)
- Analog low-pass filter (ω_k) (SINTEF Energy)
- Assorted connection equipment

The battery life time of the prototype pulse source was measured by simply running a large series of pulse with the entire system powered from the prototype's battery. This was done by rewriting the sequence control script so that for each push of the fire button, the system produced a large series of shots with a delay of 30 seconds between each shot. For each shot, the capacitor bank is not fully charged, but to an estimated mean value of 75.0 V. This results in a current pulse with an amplitude of approximately 2000 A. To provide a conducting path for the current pulse to flow, the connection cables were spread out and short circuited in the end, forming a large ring. The DAQ-Card did not do any form of sampling during this test, since measurements prior to these showed that sampling only increased the DAQ-card's load current with 1 mA per channel. The load current of the DAQ-card was found to be 0.39 A.

If the battery voltage starts to decline, as is what happens when the battery capacity is nearing depletion, the time it takes to charge the capacitor bank starts to incline. Since the voltage characteristic of a lithium-ion battery is very flat this incline in the charging time only happens when the battery's state of charge is almost at depletion, and the effects on the charging time is then very obvious. Thus, the incline in charging time is measured by visual inspection.

The digital multimeter was used to measure the load current of the DAQ-Card during the measurements. An illustration of the battery lifetime test is shown in Figure 6.1.

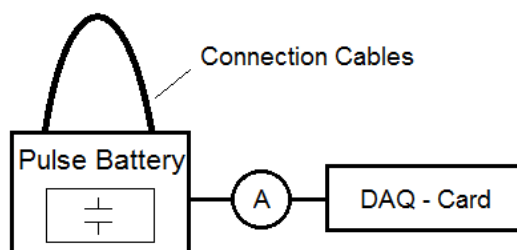


Figure 6.1: Measurement setup for the battery life time test.

6.1.2 Results and Discussion

As stated in Section 4.3.2, the pulse source needs to be able to produce at least 200 consecutive shots before being recharged. Thus, for the initial series of shots the sequence control script was programmed to perform 200 shots with a delay of 30 seconds between each shot. Meaning that the device is powered on for 1 hour and 40 minutes, while performing 200 shots.

As expected, the prototype handled this test very well. After the initial test the prototype showed no signs of increase in the capacitor bank's charging time. Hence, the prototype was put under same the test a second time.

During the second session the prototype was observed after 100 shots and then again after 150. This was done do see if any increase in the capacitor bank charging time became visual during the test. After the prototype had finished the second session, meaning a total of 400 shots and a run time of 3 hours and

20 minutes, there were still no visual increase in the capacitor charging time. While observing the setup after 150 shots it was noticed that the DAQ-Card had entered some sort of standby mode. This meaning that the load current was almost halved. After the second session the DAQ-card was reset, which increased the DAQ-card's load current back to the nominal value. Since there were no visual indication of battery depletion. A third and final session with 100 shots was conducted.

After the third session the tests were concluded. The pulse source prototype showed no indication of battery depletion even after 500 consecutive shots and a total run time of 4 hours and 10 minutes. The prototype's battery capacity exceeds what is needed for a day of field testing. This is mainly due to the DAQ-Card consuming less power than expected. The results from the test are presented in Table 6.1.

Table 6.1: Results from the battery capacity test.

<i>Number of Shots</i>	<i>Charging Voltage</i>	<i>DAQ Current</i>	<i>Total Run time</i>
500	75.0 V	0.3 A	4 h 10 min

6.2 Setpoint Accuracy

When performing condition assessment measurements it is necessary to perform repeated measurements with the same current pulse amplitude to investigate if alterations in the resistance have occurred due to softening or melting of the contact spots. It is therefore important that the prototype's setpoint adjustment is able to reproduce the same current pulse amplitude, for the same setpoint. The setpoint accuracy test looks into how well the prototype is able to reproduce the same current pulse amplitude for the same setpoint value.

6.2.1 Equipment and Measurement Setup

To perform the setpoint accuracy measurements the following equipment, in addition to the pulse source prototype with connection cables, was needed;

- Computer with Test Point software able to capture and process the measurements (Panasonic Toughbook) (P07-1320)

- DAQ-Card with two inputs, and external trigger (National Instruments USB-6251 M) (G05-0153)
- Analog low-pass filter (ω_k) (SINTEF Energy)
- Rogowski coil with current transducer ($I_{max} = 6000$ A) (PEM CWT-30R) (I04-0421)
- Coaxial Cables
- Assorted connection equipment

The setpoint accuracy test is set up almost identical to the condition assessment tests described in Section 5.2.2. The difference is that the connection cables are not connected to a line connector, but short circuited like in the setup described in Section 6.1.1. In addition there is no voltage measurement, since the purpose of the test is to see how well the pulse source prototype is able to produce the same current pulse amplitude for the same setpoint. An illustration of the measurement setup is presented in Figure 6.2.

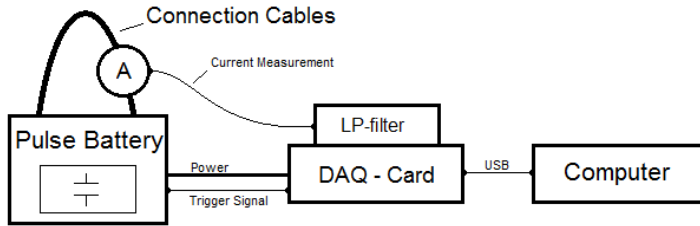


Figure 6.2: Setpoint accuracy measurement setup.

The measurements were conducted by performing four consecutive shots for five different setpoints, while recording the current amplitude for each shot. The five different setpoints chosen were: 10 V, 50 V, 100 V, 150 V, and 180 V. Though the pulse source has a capacity to create current pulses with an even greater amplitude, the Rogowski coil is not able to measure currents above 6000 A. Thus, limiting the maximum current.

6.2.2 Results and Discussion

As mentioned, it is important that the pulse source prototype is able to reproduce the same current amplitude for the same charging voltage set point. The measured current pulse amplitude of four consecutive pulses for five different setpoints is presented in Table 6.2. The table also presents the standard deviation for each setpoint. Note that the standard deviation increases as the setpoint increases. This is most likely caused by an increased leakage current at high capacitor bank voltages. Since there is an almost constant physical time delay in the control sequence, and the increased leakage current increases the reduction in the capacitor bank voltage, it becomes more difficult for the control sequence to fire at the precisely same voltage level. Therefore, creating larger deviations in the measured current for equal setpoints.

Table 6.2: Results from the battery capacity test.

<i>Set-point</i>	<i>Measured Current Amplitude [A]</i>				<i>Standard Deviation [A]</i>
	<i>1</i>	<i>2</i>	<i>3</i>	<i>4</i>	
<i>10 V</i>	311.5	319.8	309.0	318.3	5.2
<i>50 V</i>	1515.4	1510.8	1493.6	1512.8	9.9
<i>100 V</i>	2983.7	3004.9	2984.8	2949.0	23.2
<i>150 V</i>	4499.9	4492.4	4540.1	4510.9	20.9
<i>180 V</i>	5440.9	5443.8	5395.1	5454.9	26.4

The measurements show that the prototype's sequence control is able to accurately reproduce the same current amplitude for the same setpoint.

6.3 Alteration to the Prototype Design

Both the condition assessment test and functionality test showed that the pulse source prototype functioned as intended. Thus, no alterations are needed based on these results. During the condition assessment test described in Chapter 5 a small design flaw was discovered. At low setpoints the physical delay in the control sequence results in an overshoot in the charge voltage. This overshoot is relatively small, but at low capacitor bank voltages the leakage current is also low. Since the control sequence is designed to wait until the capacitor voltage is reduced to the setpoint before firing, the result is that the user must wait an extensive amount of time before the shot is fired.

To improve upon this, the control sequence script was altered to try to regulate the capacitor bank voltage by pulse width modulation (PWM) for setpoint values below 25 V. This was done by the microcontroller calculating the necessary pulse width to give the desired capacitor voltage and then using the remote shut down of the DC-DC converter to produce the required voltage pulses.

Tests on this setup showed that delays in the DC-DC converter resulted in a non-satisfactory result. The charging of the capacitor bank became slow, and the voltage did not stabilize at the desired level. Thus, a combination of the old and new control scheme was chosen. For setpoints including and below 25 V the control sequence slows the charging by switching the DC-DC converter on and off. The microcontroller then shuts off the DC-DC converter when the desired capacitor bank voltage is reached. This still produces a slight overshoot, but the slowed charging rate reduces the overshoot extensively. Hence, considerably reducing the time the user needs to wait before a shot is fired.

The changes mentioned above are included in the documentation presented in Appendix C.

7 Conclusion and Further Work

This chapter gives a summary to the most important findings of the thesis and discusses different possibilities in the further development of the pulse source prototype.

7.1 Conclusion

The aim of this thesis was to design, construct and test a new lightweight current pulse source based on weight reduction by reduced current pulse rise time and reduced connection cable cross section. Based on this, a set of five objectives were listed in Section 1.2. From these, a final conclusion to the results and discussions can be drawn.

1. The thesis shows that the final design of the prototype pulse source, by applying a 10 mF capacitor, has a weight of 7.6 kg. This is a weight loss of almost 28 kg compared to the present pulse source. The size is also substantially reduced.
2. Comparison of the condition assessment test performed by the pulse source prototype and the previous pulse source on the French Connectors shows that condition assessments correlate and are conclusive for all measurements. In addition, it was revealed that the overall measured resistance in almost consequently larger with the prototype setup. The measurements show that this is not solely caused by a reduction in the rise time.
3. The results from the condition assessment of the Finnish Connectors show that the prototype pulse source operates as intended during mass testing of connectors with an unknown condition. The measurements show that the setup has a measurement error at low current magnitudes. No conclusion was found to this phenomena and it should be investigated further as it may result in faulty condition assessments.
4. The battery lifetime measurements show that the prototype's battery capacity is able to produce 500 consecutive shots and operate continuously for 4 hours and 10 min. The setpoint accuracy test indicated that the prototype's sequence control was able to accurately produce and reproduce the same current amplitude for the same setpoint.
5. An alteration to the pulse source prototype's capacitor charging scheme was introduced to allow a faster firing sequence at low setpoints. This was

done by switching the DC-DC converter on and off to slow the charging and thereby reduce the capacitor bank voltage overshoot.

7.2 Further Work

If the pulse source prototype is to be developed further there are several aspects to the design and measurement technique that needs to be revised.

The condition assessment measurements show that the current configuration has a measurement error at low current magnitudes. The error is most prominent for connectors in a very good condition, but is most likely present in all measurements. For connectors in good and poor condition this error could cause a faulty assessment. Thus, it is important that further study is put into this subject to try and locate the source of the error.

With the introduction of a software based control sequence, it would be possible to create a fully automated measurement process. Though, the microcontroller included in this version of the prototype has some limitation with regards to sampling and post processing, there are commercially available microcontrollers that have the processing power to perform both sampling and post processing of the measurements. Hence, a fully automated system, which performs the required measurements, and returns a conclusion to the condition of the connector with the press of a button should be possible.

A reduced capacitor bank requires an increased charging voltage to create the same current magnitudes. An increased charging voltage increases the contact hazard, thus increasing the risk of operation. Further studies should therefore be conducted to look into how the risk of operation could be reduced.

It is also important that further tests on different line connectors are made to increase the validity of the method. A field test should also be conducted to reveal problems to the pulse source prototype not apparent in laboratory tests.

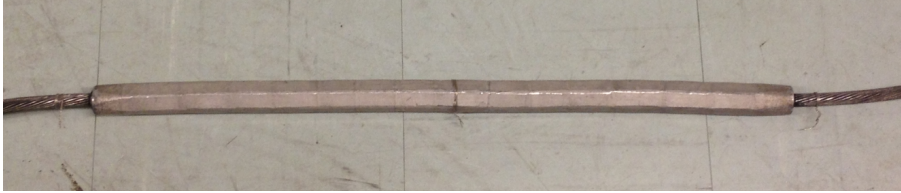
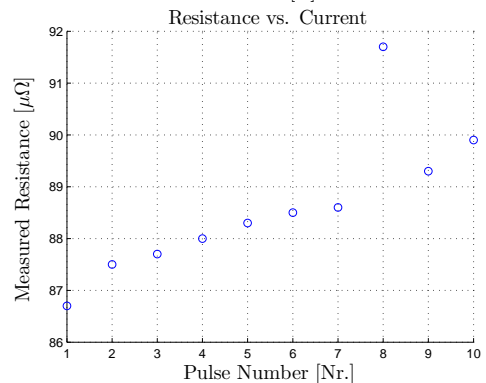
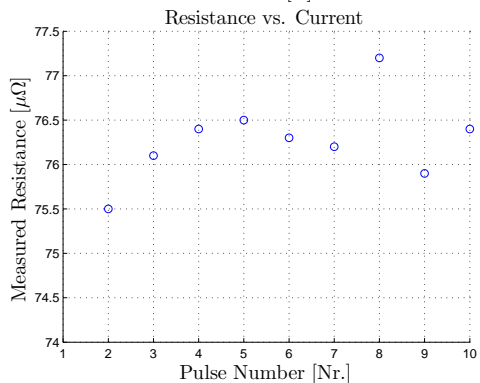
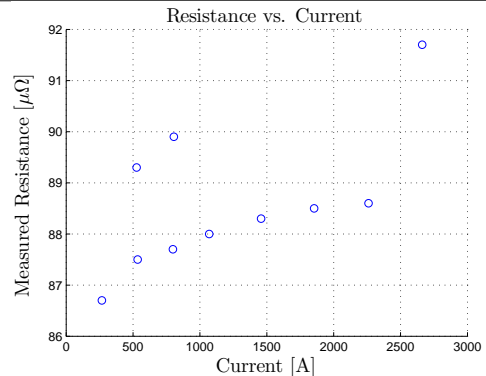
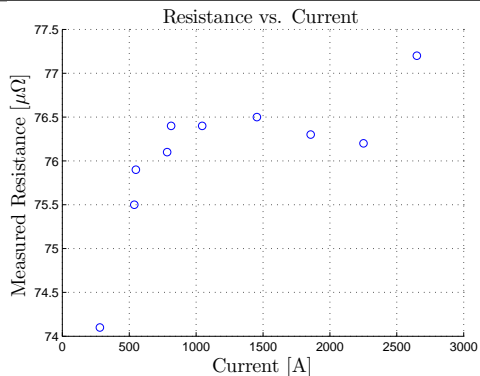
References

- [1] S. Refsnæs, H. Jensvold, and O. Rørvik, *Tilstandskontroll av klemmer og skjøter i kraftledninger*. SINTEF Energy Research, November 2000. Technica Report.
- [2] M. Runde, *Current Interruption in Power Grids*. Norwegian University of Science and Technology, 2013. Compendium.
- [3] R. Holm, *Electric Contacts - Theory and Application*. Berlin: Springer, fourth ed., 1967.
- [4] B. W. Callen, B. Johnson, P. King, R. S. Timsit, and W. H. Abbott, *Environmental Degradation of Utility Power Connectors in a Harsh Environment*. Pittsburgh, PA, USA: Electrical Contacts, 1999. Proceedings of the Forty-Fifth IEEE Holm Conference, 1999.
- [5] M. Runde, S. M. Hellesø, K. Halsan, J. Pestourie, C. Spelleman, and B. Colomb, *Pulse Current Measurements for Condition Assessment of Conductor Joints of Overhead Lines*. Cigre, 2008. Technical Report.
- [6] M. Runde, *In Material Transport and Related Interfacial Phenomena in Stationary Aluminium Contacts*. Norges Tekniske Høgskole, 1987. Doktor Ingeniøravhandling.
- [7] K. Fandrem, *Condition Assessment of Line Connectors by Current Pulse Measurements - Effect of Reduced Pulse Rise Time and Connection Cable Cross Section*. Trondheim, Norway: Norwegian University of Science and Technology, 2013. Specialization Project.
- [8] R. S. Timsit, *Origin, Detection and Cost of Connector Degradation in Electrical Transmission and Distribution Systems*. Suzhou, China: Proc. of the First Int. Conf. on Reliability of Electrical Products and Electrical Contacts, 2004.
- [9] M. Runde and S. M. Hellesø, *Line Joints Removed From Service in the French Grid*. SINTEF Energy Research, Desember 2006. Project Memo (Confidential).
- [10] J. Harold J. Ruhl, *Spreading Velocity of the Active Area Boundary in a Thyristor*. IEEE, September 1970. IEEE Transactions on Electron Devices, Volume:17 , Issue: 9.

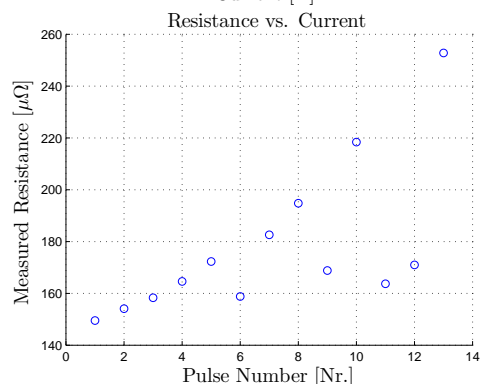
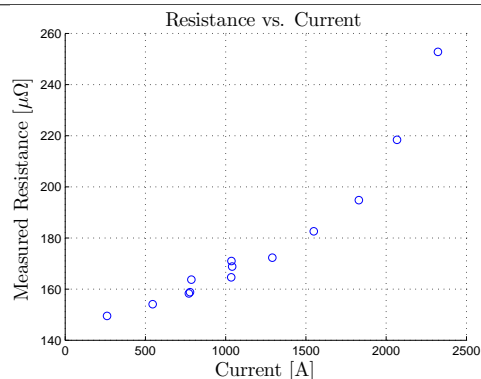
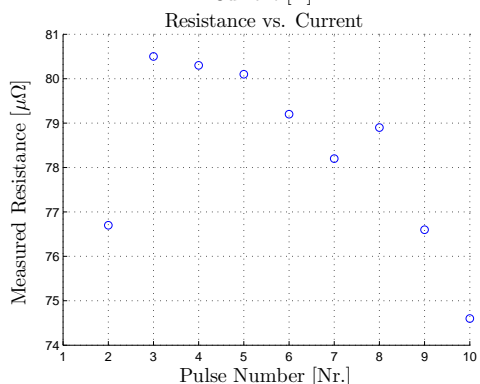
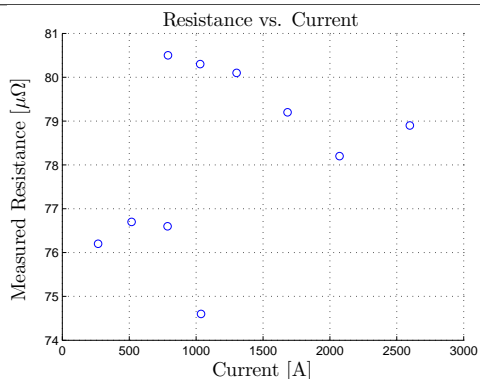
- [11] P. Electronics, "Pq-series datasheet." <http://www.picoelectronics.com/dcdclow/peQP.htm>. Accessed: 23-04-2014.
- [12] S. R. Holsdal, *Tilstandskontroll av lineskjøter*. Norges teknisk-naturvitenskaplig universitet - Institutt for elkraftteknikk, 2006. Master Thesis.

Appendix A

- *Condition Assessment* -

French Connector No. 1*Conductor diameter:* 20.5mm*Current measurement:* Rogowski-coil*Current pulse source:* Light weight prototype*Strand layers:* 3 Fe + 1Al*Condition:* Apparently dry conductor with a moderately corroded surface.*Longer conductor side:**Shorter conductor side:**Current Pulse Measurements (R [$\mu\Omega$])**Comments:* The longer conductor side show almost no change in resistance for the entire area tested.*Comments:* The short conductor side show a slight, but insignificant increase in the resistance for low currents.*Conclusion:*

Both sides seem to be in a very good condition. The short conductor side is in a some what poorer state than the longer conductor side.

Line Connector No. 6*Conductor diameter:* 20.5mm*Current measurement:* Rogowski-coil*Current pulse source:* Light weight prototype*Strand layers:* 3 Fe + 1Al*Condition:* Apparently dry conductor with a rather corroded surface.*Longer conductor side:**Shorter conductor side:**Current Pulse Measurements (R [$\mu\Omega$])*


Comments: The longer side shows an almost constant R for the entire current range tested.

Comments: The short conductor side shows slight increase over the entire current area tested, and is not reversible after about 1500 A.

Conclusion:

The longer conductor side is in a very good condition.

The shorter conductor side is in a poor condition.

French Connector No. 11		
<p>Conductor diameter: 20.5mm Current measurement: Rogowski-coil Current pulse source: Light weight prototype</p>	<p>Strand layers: 3 Fe + 1Al Condition: Apparently dry conductor with a rather corroded surface.</p>	
		
	<p><i>Longer conductor side:</i></p>	<p><i>Shorter conductor side:</i></p>
<p><i>Current Pulse Measurements (R [$\mu\Omega$])</i></p>	<p>N/A</p>	
<p><i>Comments:</i> The longer conductor side shows a small increase in the resistance for low currents, and a steady incline after 500 A. Melting occurs at about 2000 A.</p>	<p><i>Comments:</i> The shorter conductor side was not tested due to a mechanical error on the connector barrel.</p>	
<p><i>Conclusion:</i> The longer conductor side is in a good condition.</p>		

Finnish Connector No. 1																																																												
<i>Conductor type:</i> Ostrich <i>Current measurement:</i> Rogowski-coil <i>Current pulse source:</i> Light weight prototype	<i>Strand layers:</i> 2 Fe + 2 Al <i>Condition:</i> Apparently dry conductor with a slightly polluted surface.																																																											
	<i>Connector Side A:</i>	<i>Connector Side B:</i>																																																										
R_{DC} [$\mu\Omega$]	<i>Before:</i> N/A <i>After:</i> N/A	<i>Before:</i> N/A <i>After:</i> N/A																																																										
	<i>Conductor Side A:</i>	<i>Conductor Side B:</i>																																																										
Current Pulse Measurements (R [$\mu\Omega$])	<p style="text-align: center;">Resistance vs. Current</p> <table border="1"> <caption>Approximate data for Side A Resistance vs. Current</caption> <thead> <tr><th>Current [A]</th><th>Measured Resistance [$\mu\Omega$]</th></tr> </thead> <tbody> <tr><td>1000</td><td>70</td></tr> <tr><td>1500</td><td>70</td></tr> <tr><td>2500</td><td>75</td></tr> <tr><td>3800</td><td>79</td></tr> <tr><td>5500</td><td>87</td></tr> </tbody> </table> <p style="text-align: center;">Resistance vs. Current</p> <table border="1"> <caption>Approximate data for Side A Resistance vs. Pulse Number</caption> <thead> <tr><th>Pulse Number [Nr.]</th><th>Measured Resistance [$\mu\Omega$]</th></tr> </thead> <tbody> <tr><td>1</td><td>70</td></tr> <tr><td>2</td><td>70</td></tr> <tr><td>3</td><td>75</td></tr> <tr><td>4</td><td>79</td></tr> <tr><td>5</td><td>87</td></tr> </tbody> </table>	Current [A]	Measured Resistance [$\mu\Omega$]	1000	70	1500	70	2500	75	3800	79	5500	87	Pulse Number [Nr.]	Measured Resistance [$\mu\Omega$]	1	70	2	70	3	75	4	79	5	87	<p style="text-align: center;">Resistance vs. Current</p> <table border="1"> <caption>Approximate data for Side B Resistance vs. Current</caption> <thead> <tr><th>Current [A]</th><th>Measured Resistance [$\mu\Omega$]</th></tr> </thead> <tbody> <tr><td>1000</td><td>41.3</td></tr> <tr><td>2500</td><td>41.4</td></tr> <tr><td>4000</td><td>41.0</td></tr> <tr><td>5500</td><td>41.2</td></tr> <tr><td>5500</td><td>41.6</td></tr> <tr><td>5800</td><td>41.6</td></tr> <tr><td>5800</td><td>41.8</td></tr> </tbody> </table> <p style="text-align: center;">Resistance vs. Current</p> <table border="1"> <caption>Approximate data for Side B Resistance vs. Pulse Number</caption> <thead> <tr><th>Pulse Number [Nr.]</th><th>Measured Resistance [$\mu\Omega$]</th></tr> </thead> <tbody> <tr><td>1</td><td>41.8</td></tr> <tr><td>2</td><td>41.3</td></tr> <tr><td>3</td><td>41.4</td></tr> <tr><td>4</td><td>41.0</td></tr> <tr><td>5</td><td>41.2</td></tr> <tr><td>6</td><td>41.6</td></tr> <tr><td>7</td><td>41.6</td></tr> <tr><td>8</td><td>41.8</td></tr> </tbody> </table>	Current [A]	Measured Resistance [$\mu\Omega$]	1000	41.3	2500	41.4	4000	41.0	5500	41.2	5500	41.6	5800	41.6	5800	41.8	Pulse Number [Nr.]	Measured Resistance [$\mu\Omega$]	1	41.8	2	41.3	3	41.4	4	41.0	5	41.2	6	41.6	7	41.6	8	41.8
Current [A]	Measured Resistance [$\mu\Omega$]																																																											
1000	70																																																											
1500	70																																																											
2500	75																																																											
3800	79																																																											
5500	87																																																											
Pulse Number [Nr.]	Measured Resistance [$\mu\Omega$]																																																											
1	70																																																											
2	70																																																											
3	75																																																											
4	79																																																											
5	87																																																											
Current [A]	Measured Resistance [$\mu\Omega$]																																																											
1000	41.3																																																											
2500	41.4																																																											
4000	41.0																																																											
5500	41.2																																																											
5500	41.6																																																											
5800	41.6																																																											
5800	41.8																																																											
Pulse Number [Nr.]	Measured Resistance [$\mu\Omega$]																																																											
1	41.8																																																											
2	41.3																																																											
3	41.4																																																											
4	41.0																																																											
5	41.2																																																											
6	41.6																																																											
7	41.6																																																											
8	41.8																																																											
	<i>Comments:</i> Connector side A shows no increase in the resistance below 1500 A. The resistance increases slightly past this point.	<i>Comments:</i> Connector side B shows little or no increase in the resistance with increasing current.																																																										
	<i>Conclusion:</i> Connector side A is in a good condition. Connector side B is in a very good condition.																																																											

Finnish Connector No. 2	
<i>Conductor type:</i> Ostrich <i>Current measurement:</i> Rogowski-coil <i>Current pulse source:</i> Light weight prototype	<i>Strand layers:</i> 2 Fe + 2 Al <i>Condition:</i> Apparently dry conductor with a slightly polluted surface.
	<i>Connector Side A:</i>
R_{DC} [$\mu\Omega$]	<i>Before:</i> 46.3 <i>After:</i> N/A
	<i>Connector Side B:</i>
	<i>Before:</i> 74.4 <i>After:</i> 81.3
<i>Current Pulse Measurements (R [$\mu\Omega$])</i>	<div style="display: flex; justify-content: space-around;"> <div style="width: 45%;"> <p style="text-align: center;">Resistance vs. Current</p> </div> <div style="width: 45%;"> <p style="text-align: center;">Resistance vs. Current</p> </div> </div>
	<div style="display: flex; justify-content: space-around;"> <div style="width: 45%;"> <p style="text-align: center;">Resistance vs. Current</p> </div> <div style="width: 45%;"> <p style="text-align: center;">Resistance vs. Current</p> </div> </div>
	<p><i>Comments:</i> Connector side A shows little to no increase in the resistance for currents below 2000 A. For currents higher than this the resistance increases in a reversible manner.</p>
	<p><i>Comments:</i> Connector side B shows a slight increase in the resistance for currents below 1250 A. After this the resistance increases rapidly in a reversible manner before melting occurs at about 3000 A.</p>
<p><i>Conclusion:</i> Connector side A is found to be in a good condition, while connector side B is in a poor condition.</p>	

Finnish Connector No. 3		
<i>Conductor type:</i> Ostrich <i>Current measurement:</i> Rogowski-coil <i>Current pulse source:</i> Light weight prototype	<i>Strand layers:</i> 2 Fe + 2 Al <i>Condition:</i> Apparently dry conductor with a slightly polluted surface.	
	<i>Connector Side A:</i>	
R_{DC} [$\mu\Omega$]	<i>Before:</i> 32.9 <i>After:</i> 33.6	
	<i>Connector Side B:</i>	
	<i>Before:</i> 31.7 <i>After:</i> 31.9	
<i>Current Pulse Measurements (R [$\mu\Omega$])</i>	Resistance vs. Current 	Resistance vs. Current
	Resistance vs. Current 	Resistance vs. Current
<i>Comments:</i> Connector side A shows little or no increase in the resistance with increasing current for the entire test range.		
<i>Comments:</i> Connector side B shows a small increase in the current for values below 1500A. For higher currents the resistance shows almost no change.		
<i>Conclusion:</i> Both connector sides are in a very good condition.		

Finnish Connector No. 4	
<i>Conductor type:</i> Ostrich <i>Current measurment:</i> Rogowski-coil <i>Current pulse source:</i> Light weight prototype	<i>Strand layers:</i> 2 Fe + 2 Al <i>Condition:</i> Apparently dry conductor with a slightly polluted surface.
	<i>Connector Side A:</i>
R_{DC}	<i>Before:</i> 50.1 <i>After:</i> 50.4
$[\mu\Omega]$	<i>Before:</i> 56.5 <i>After:</i> 58.8
<i>Current Pulse Measurements (R [$\mu\Omega$])</i>	
<i>Comments:</i> Connector side A shows a slight increase in the resistance up to about 1000A before stabilizing. After 2500 A the resistance starts to increase in a reversible manner with increasing current.	
<i>Comments:</i> Connector side B also shows an increase in the resistance for low currents before stabilizing. The resistance increases in a reversible manner from 2000 A, before melting occurs at 4750 A	
<i>Conclusion:</i> Both connector sides are in a good conditon.	

Finnish Connector No. 5	
<i>Conductor type:</i> Ostrich <i>Current measurement:</i> Rogowski-coil <i>Current pulse source:</i> Light weight prototype	<i>Strand layers:</i> 2 Fe + 2 Al <i>Condition:</i> Apparently dry conductor with a slightly polluted surface.
<i>Connector Side A:</i>	<i>Connector Side B:</i>
R_{DC} $[\mu\Omega]$	
<i>Before:</i> 51.0 <i>After:</i> 51.0	<i>Before:</i> 71.0 <i>After:</i> 113.9
<i>Current Pulse Measurements (R [$\mu\Omega$])</i>	
<i>Comments:</i> Connector side A shows a slight increase in the resistance for low currents up to about 1000 A. After 2500 A the resistance increases in a reversible manner with increasing current.	<i>Comments:</i> Connector side B shows a reversible increase in the resistance from about 1000 A until melting occurs at 2250 A
<i>Conclusion:</i> Line connector side A is in a very good condition Line connector side B is in a good condition.	

Finnish Connector No. 6	
<i>Conductor type:</i> Ostrich <i>Current measurement:</i> Rogowski-coil <i>Current pulse source:</i> Light weight prototype	<i>Strand layers:</i> 2 Fe + 2 Al <i>Condition:</i> Apparently dry conductor with a slightly polluted surface.
	<i>Connector Side A:</i>
R_{DC} [$\mu\Omega$]	<i>Before:</i> 37.4 <i>After:</i> 37.5
	<i>Connector Side B:</i>
	<i>Before:</i> 86.7 <i>After:</i> 83.9
Current Pulse Measurements (R [$\mu\Omega$])	<div style="display: flex; justify-content: space-around;"> <div style="width: 45%;"> <p style="text-align: center;">Resistance vs. Current</p> </div> <div style="width: 45%;"> <p style="text-align: center;">Resistance vs. Current</p> </div> </div>
	<div style="display: flex; justify-content: space-around;"> <div style="width: 45%;"> <p style="text-align: center;">Resistance vs. Current</p> </div> <div style="width: 45%;"> <p style="text-align: center;">Resistance vs. Current</p> </div> </div>
	<p><i>Comments:</i> Connector side A shows little or no increase in the resistance for the entire current range tested.</p>
	<p><i>Comments:</i> Connector side B shows a steady increase in the resistance already at low currents. The resistance increases in a reversible manner until melting occurs at 3500 A.</p>
	<p><i>Conclusion:</i> Connector side A is in a very good condition Connector side B is in a poor condition.</p>

Finnish Connector No. 7	
<i>Conductor type:</i> Ostrich <i>Current measurement:</i> Rogowski-coil <i>Current pulse source:</i> Light weight prototype	<i>Strand layers:</i> 2 Fe + 2 Al <i>Condition:</i> Apparently dry conductor with a slightly polluted surface.
	<i>Connector Side A:</i>
R_{DC} [$\mu\Omega$]	<i>Before:</i> 39.6 <i>After:</i> 39.2
	<i>Connector Side B:</i>
	<i>Before:</i> 50.5 <i>After:</i> 50.8
Current Pulse Measurements (R [$\mu\Omega$])	<div style="display: flex; justify-content: space-around;"> <div style="width: 45%;"> <p style="text-align: center;">Resistance vs. Current</p> </div> <div style="width: 45%;"> <p style="text-align: center;">Resistance vs. Current</p> </div> </div> <div style="display: flex; justify-content: space-around; margin-top: 10px;"> <div style="width: 45%;"> <p style="text-align: center;">Resistance vs. Current</p> </div> <div style="width: 45%;"> <p style="text-align: center;">Resistance vs. Current</p> </div> </div>
<i>Comments:</i>	Connector side A shows little to no increase in the resistance for increasing current over the entire range tested.
<i>Conclusion:</i>	Connector side B shows an increase in the resistance for low currents before stabilizing at around 1000 A. After 2500 A the resistance starts to increase in a reversible manner.
Connector side A is in a very good condition. Connector side B is in a good condition.	

Finnish Connector No. 8	
<i>Conductor type:</i> Ostrich <i>Current measurement:</i> Rogowski-coil <i>Current pulse source:</i> Light weight prototype	<i>Strand layers:</i> 2 Fe + 2 Al <i>Condition:</i> Apparently dry conductor with a slightly polluted surface.
	<i>Connector Side A:</i>
R_{DC} [$\mu\Omega$]	<i>Connector Side B:</i>
	<i>Before:</i> 34.8 <i>After:</i> 34.8
	<i>Before:</i> 73.5 <i>After:</i> 65.5
<i>Current Pulse Measurements (R [$\mu\Omega$])</i>	<div style="display: flex; justify-content: space-around;"> <div style="width: 45%;"> <p style="text-align: center;">Resistance vs. Current</p> </div> <div style="width: 45%;"> <p style="text-align: center;">Resistance vs. Current</p> </div> </div> <div style="display: flex; justify-content: space-around; margin-top: 10px;"> <div style="width: 45%;"> <p style="text-align: center;">Resistance vs. Current</p> </div> <div style="width: 45%;"> <p style="text-align: center;">Resistance vs. Current</p> </div> </div>
<p><i>Comments:</i> Connector side A shows little to no increase in the resistance for increasing current over the entire range tested.</p>	
<p><i>Comments:</i> Connector side B shows an reversible increase in the resistance after about 1750 A. Melting occurs at about 5000 A.</p>	
<p><i>Conclusion:</i> Connector side A is in a very good condition Connector side B is in a good condition.</p>	

Finnish Connector No. 9	
<i>Conductor type:</i> Ostrich <i>Current measurement:</i> Rogowski-coil <i>Current pulse source:</i> Light weight prototype	<i>Strand layers:</i> 2 Fe + 2 Al <i>Condition:</i> Apparently dry conductor with a slightly polluted surface.
	<i>Connector Side A:</i>
R_{DC} [$\mu\Omega$]	Before: 32.0 After: 32.3
<i>Current Pulse Measurements (R [$\mu\Omega$])</i>	<div style="display: flex; justify-content: space-around;"> <div style="width: 45%;"> <p style="text-align: center;">Resistance vs. Current</p> </div> <div style="width: 45%;"> <p style="text-align: center;">Resistance vs. Current</p> </div> </div>
	<i>Connector Side B:</i>
	Before: 49.8 After: 49.7
	<div style="display: flex; justify-content: space-around;"> <div style="width: 45%;"> <p style="text-align: center;">Resistance vs. Current</p> </div> <div style="width: 45%;"> <p style="text-align: center;">Resistance vs. Current</p> </div> </div>
	<i>Comments:</i> Connector side A shows almost no increase in the resistance for the entire current range tested.
	<i>Comments:</i> Connector side B shows a slight increase in the resistance with increasing current after 2500 A.
	<i>Conclusion:</i> Both connector sides are in a very good condition, but side A is in a somewhat better condition than side B.

Finnish Connector No. 10	
<i>Conductor type:</i> Ostrich <i>Current measurement:</i> Rogowski-coil <i>Current pulse source:</i> Light weight prototype	<i>Strand layers:</i> 2 Fe + 2 Al <i>Condition:</i> Apparently dry conductor with a slightly polluted surface.
	<i>Connector Side A:</i>
R_{DC} [$\mu\Omega$]	<i>Before:</i> 109.6 <i>After:</i> 116.9
	<i>Connector Side B:</i>
	<i>Before:</i> 119.3 <i>After:</i> 127.8
<i>Current Pulse Measurements (R [$\mu\Omega$])</i>	<div style="display: flex; justify-content: space-around;"> <div style="width: 45%;"> <p style="text-align: center;">Resistance vs. Current</p> </div> <div style="width: 45%;"> <p style="text-align: center;">Resistance vs. Current</p> </div> </div> <div style="display: flex; justify-content: space-around; margin-top: 20px;"> <div style="width: 45%;"> <p style="text-align: center;">Resistance vs. Current</p> </div> <div style="width: 45%;"> <p style="text-align: center;">Resistance vs. Current</p> </div> </div>
<i>Comments:</i>	<p>Connector side A shows an reversible increase in the resistance even for low currents, before melting occurs somewhere past 2000 A.</p>
<i>Conclusion:</i>	<p>Both connector sides are in a poor condition, but side B is in a somewhat poorer condition than side A.</p>

Appendix B

- *Microcontroller Script* -

```

#include <LiquidCrystal.h>
//Final version of the current pulse source prototype sequence control.
//Build date: 08.05.2014

//Defining LCD-panel pins:
LiquidCrystal lcd(12, 11, 8, 7, 6, 5);

//Variables:
double voltlvl = 0; //Variable which calculates and stores the actual voltage level.
int rdyfire = 0; //Variable indicating that the system is ready to charge.
int sequence = 0; //Used to indicate fire sequence.
int buttonstate = 0; //Variable storing the fire button state.
int n = 0; //Used to initiate boot sequence.
int k = 0; //Used to differentiate between PWM charging and regular charging.
int pwm = 64; //Pulse width.

//Outputs:
int voltpin = 0; //Voltage input (A0)
int rotpot = 1; //Setpoint input (A1)
int DAQtrigg = 3; //DAQ trigger signal.
int fire = 4; //Thyristor trigger signal.
int pinshutdown = 9; //Signal for DC/DC-converter remote shutdown.
int pinexbias = 10; //Signal for DDC/DC-converter ext. bias.
int button = 13; //Trigger Button pin

void setup() {
  Serial.begin(9600);
  lcd.begin(16, 2);

  //Defining if the the digital IO is and input or output.
  pinMode(pinshutdown, OUTPUT);
  pinMode(pinexbias, OUTPUT);
  pinMode(fire, OUTPUT);
  pinMode(DAQtrigg, OUTPUT);
  pinMode(button, INPUT);
}

void loop() {
  //Initial conditions:
  digitalWrite(pinshutdown, HIGH);
  digitalWrite(pinexbias, LOW);

  //Boot sequence in lcd display:
  while (millis() < 5000){
    lcd.setCursor(0,0);
    lcd.print("Pulse_Src_v.1.0");
    lcd.setCursor(0,1);
    lcd.print("Initializing");
    delay(500);
    lcd.setCursor(0,1);
    lcd.print("Initializing.");
    delay(500);
    lcd.setCursor(0,1);
    lcd.print("Initializing..");
    delay(500);
    lcd.setCursor(0,1);
    lcd.print("Initializing...");
    delay(500);
    lcd.clear();
  }
}

```



```

}

if (n == false){
  lcd.clear();
  n = 1;
}

//Outer Sequence (Level 1):
double setpoint = analogRead(rotpot);
double voltlvl = analogRead(voltpin);
delay(50);

lcd.setCursor(0,0);
lcd.print("Vchg:");
lcd.print(voltlvl/1023*303.8,1);
lcd.setCursor(0,1);
lcd.print("Vset:");
lcd.print(setpoint/1023*300,1);

buttonstate = digitalRead(button);

if(buttonstate == HIGH){
  lcd.clear();
  sequence = 1;
  delay(100);
}
//Charging Sequence (Level 2):
while (sequence == HIGH){
  digitalWrite(pinexbias ,HIGH);
  voltlvl = analogRead(voltpin);

  if (voltlvl <= setpoint){
    voltlvl = analogRead(voltpin);

    if (k == false){
      if(setpoint <= 85.0){
        analogWrite(pinshutdown ,pwm);
        delay(5);
        lcd.setCursor(0,0);
        lcd.print("PWM Charging!");
        k = 1;
      }

      if (setpoint > 85.0){
        digitalWrite(pinshutdown ,LOW);
        delay(5);
        lcd.setCursor(0,0);
        lcd.print("Charging!");
        k = 1;
      }
    }
    lcd.setCursor(0,1);
    lcd.print("Vchg:");
    lcd.print(voltlvl*303.80/1023,1);
    delay(5);
  }

  if (voltlvl >= setpoint + 2){
    digitalWrite(pinshutdown ,HIGH);
  }
}

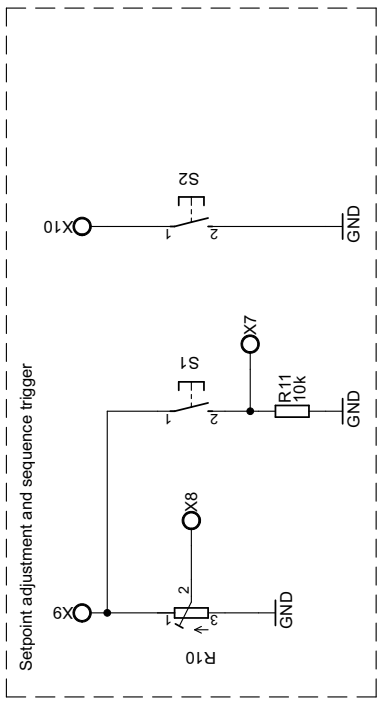
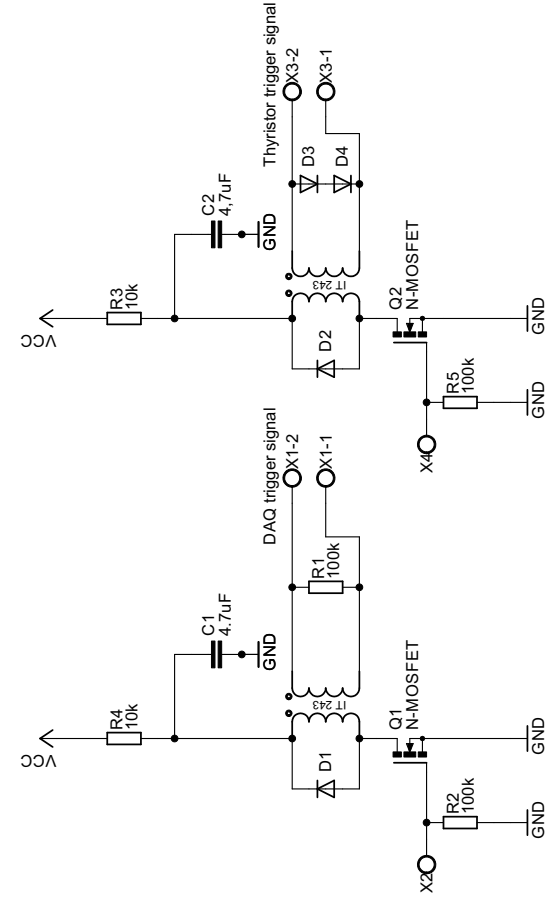
```

```
    rdyfire = 1;
    delay(1);
    lcd.clear();
}
//Firing Sequence(Level 3):
while (rdyfire == HIGH){
    voltlvl = analogRead(voltpin);
    lcd.setCursor(0,0);
    lcd.print("Fireing!");

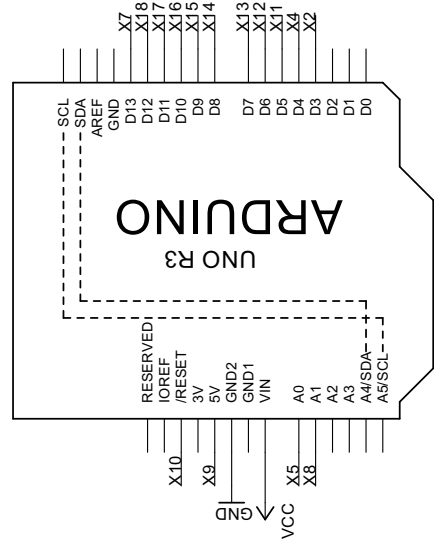
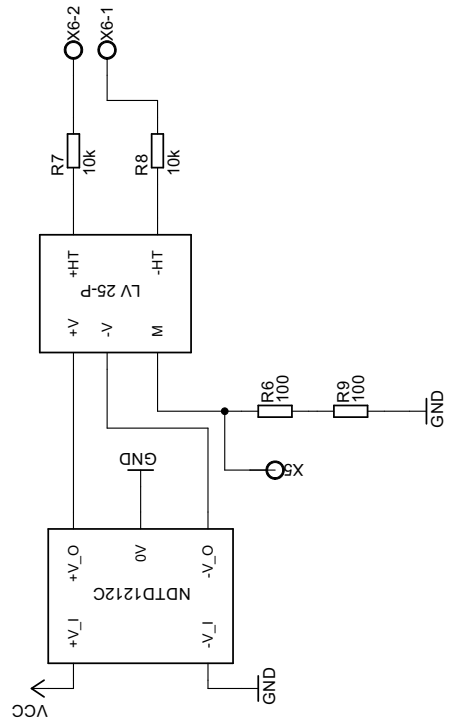
    if (voltlvl <= setpoint){
        digitalWrite(DAQtrigg,HIGH);
        //delay(1);
        digitalWrite(DAQtrigg,LOW);
        delay(1);
        digitalWrite(fire,HIGH);
        delay(5);
        digitalWrite(fire,LOW);
        rdyfire = 0;
        sequence = 0;
        k=0;
        lcd.clear();
        delay(50);
    }
    delay(1);
} // End Level 3
delay(1);
} //End Level 2
} //End Level 1
```

Appendix C

- *Circuit Schematics* -



Voltage measurement



Sintef Energy Research

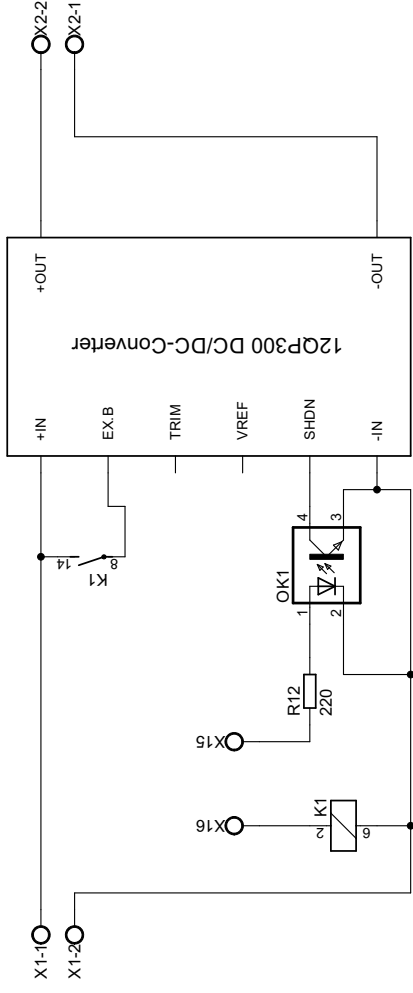
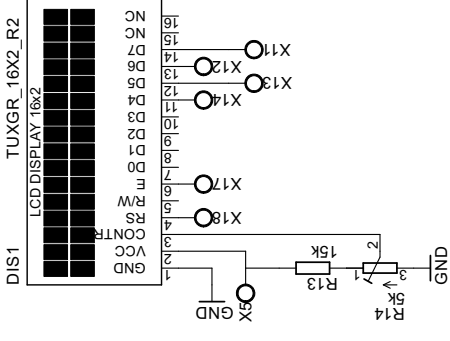
TITLE: Sequence control

Document Number:

REV:

Date: 28-05-2014 5:48:13 PM

Sheet: 1/1



Sintef Energy Research

TITLE: Sequence converter

Document Number:

REV:

Date: 28-05-2014 6:49:54 PM

Sheet: 1/1

Appendix D

- *Component List* -

Component List:

Main Circuit:

Capacitor: EPCOS B43740-A109-M 10000 $\mu\Omega$

Battery: Hy-Line Li-Ion Battery H2B182-B

Thyristor: Eupec TD330N

Main DC-DC Converter: Pico Electronics 12QP300

Opto Coupler: Sharp PC817X

Microcontroller Unit: Arduino UNO R3

Voltage Measurement Circuit:

Current Transducer: LEM LV25-P

Measurement Circuit DC-DC Converter: Murata NDTD1212C

DAQ-Card and Thyristor Trigger Signal:

Pulse Transformer: Schaffner IT232

N-Mosfet: International Rectifier IRF1018EPbF

Appendix E

- *ACSR Product Catalog* -



Avenida Francisco de Miranda, Edif. Parque Cristal, Torre Oeste
 Los Palos Grandes – Caracas 1062 - Venezuela
 Tel: +58 (212) 285-5707 Fax: +58 (212) 285-3269



PRODUCT CATALOG – ACSR (Aluminum Conductor, Steel Reinforced)

ASTM CONDUCTOR SIZES															
Code Word	Size (AWG or KCM)	Stranding (Al/St)	Diameter (inches)			Complete Cable	Weight Per 1000 ft (Lbs)			Content % Al	Rated Strength (Lbs)	Resistance ¹		Current Rating ² (Amps)	
			Indiv. Al	Wires Stl	Steel Core		Al	Stl	Total			DC @ 20 °C	AC @ 75 °C		
Turkey	6	6/1	.0661	.0661	.0661	.198	24.5	11.6	36.1	67.90	32.10	1,190	.641	.806	105
Swan	4	6/1	.0834	.0834	.0834	.250	39.0	18.4	57.4	67.90	32.10	1,860	.403	.515	140
Swanate	4	7/1	.0772	.1029	.1029	.257	39.0	28.0	67.0	58.13	41.87	2,360	.399	.519	140
Sparrow	2	6/1	.1052	.1052	.1052	.316	62.0	29.3	91.3	67.90	32.10	2,850	.254	.332	184
Sparate	2	7/1	.0974	.1299	.1299	.325	62.0	44.7	106.7	58.13	41.87	3,640	.251	.338	184
Robin	1	6/1	.1181	.1181	.1181	.354	78.2	36.9	115.1	67.90	32.10	3,550	.201	.268	212
Raven	1/0	6/1	.1327	.1327	.1327	.398	98.7	46.6	145.3	67.90	32.10	4,380	.159	.217	242
Quail	2/0	6/1	.1489	.1489	.1489	.447	124.3	58.7	183.0	67.90	32.10	5,300	.126	.176	276
Pigeon	3/0	6/1	.1672	.1672	.1672	.502	156.7	74.0	230.7	67.90	32.10	6,620	.100	.144	315
Penguin	4/0	6/1	.1878	.1878	.1878	.563	197.7	93.4	291.1	67.90	32.10	8,350	.0795	.119	357
Waxwing	266.8	18/1	.1217	.1217	.1217	.609	250.3	39.2	289.5	86.45	13.55	6,880	.0643	.0787	449
Partridge	266.8	26/7	.1013	.0788	.2364	.642	251.7	115.6	367.2	68.53	31.47	11,300	.0637	.0779	475
Ostrich	300.0	26/7	.1074	.0835	.2505	.680	282.9	129.8	412.7	68.53	31.47	12,700	.0567	.0693	492
Merlin	336.4	18/1	.1367	.1367	.1367	.683	315.8	49.5	365.2	86.45	13.55	8,680	.0510	.0625	519
Linnnet	336.4	26/7	.1137	.0884	.2652	.720	317.1	145.4	462.5	68.53	31.47	14,100	.0505	.0618	529
Oriole	336.4	30/7	.1059	.1059	.3117	.741	318.2	208.9	527.1	60.35	39.65	17,300	.0502	.0613	535
Chickadee	297.5	18/1	.1486	.1486	.1486	.743	373.1	58.5	431.6	86.45	13.55	9,940	.0432	.0529	576
Brant	397.5	24/7	.1287	.0858	.2574	.772	375.0	137.0	512.0	73.23	26.77	14,600	.0430	.0526	584
Ibis	397.5	26/7	.1236	.0961	.2883	.783	374.7	171.9	546.6	68.53	31.47	16,300	.0428	.0523	587
Lark	397.5	30/7	.1151	.1151	.3453	.806	375.8	246.8	622.6	60.35	39.65	20,300	.0425	.0519	594
Pelican	477.0	18/1	.1628	.1628	.1628	.814	447.8	70.2	518.0	86.45	13.55	11,800	.0360	.0442	646
Flicker	477.0	24/7	.1410	.0940	.2820	.846	450.1	164.4	614.5	73.23	26.77	17,200	.0358	.0439	655
Hawk	477.0	26/7	.1354	.1053	.3159	.858	449.6	206.4	656.0	68.53	31.47	19,500	.0356	.0436	659
Hen	477.0	30/7	.1261	.1261	.3783	.883	451.1	296.2	747.3	60.35	39.65	23,800	.0354	.0433	666
Osprey	556.5	18/1	.1758	.1758	.1758	.879	522.2	81.8	604.1	86.45	13.55	13,700	.0308	.0379	711
Parakeet	556.5	24/0	.1523	.1015	.3045	.914	525.1	191.7	716.9	73.23	26.77	19,800	.0307	.0376	721
Dove	556.5	26/7	.1463	.1138	.3414	.927	525.0	241.0	766.0	68.53	31.47	22,600	.0306	.0375	726
Eagle	556.5	30/7	.1362	.1362	.4086	.953	526.3	345.6	871.8	60.35	39.65	27,800	.0303	.0372	734
Peacock	605.0	24/7	.1588	.1059	.3177	.953	570.9	208.7	779.6	73.23	26.77	21,600	.0282	.0346	760
Squab	605.0	26/7	.1525	.1186	.3558	.966	570.4	261.8	832.2	68.53	31.47	24,300	.0281	.0345	765
Wood Duck	605.0	30/7	.1420	.1420	.4260	.994	572.0	375.6	947.7	60.35	39.55	28,900	.0279	.0342	774
Teal	605.0	30/19	.1420	.0852	.4260	.994	572.0	367.4	939.4	60.89	39.11	30,000	.0279	.0342	773
Kingbird	636.0	18/1	.1880	.1880	.1880	.940	597.2	93.6	690.8	86.45	13.55	15,700	.0270	.0332	773
Swift	636.0	36/1	.1329	.1329	.1329	.930	596.9	46.8	643.7	92.80	7.20	13,800	.0271	.0334	769
Rook	636.0	24/7	.1628	.1085	.3255	.977	600.0	219.1	819.1	73.23	26.77	22,600	.0268	.0330	784